Exploring HONO production from particulate nitrate photolysis in Chinese representative regions: characteristics, influencing factors and environmental implications

Bowen Li[1], Jian Gao[1], Chun Chen[1], Liang Wen[1], Yuechong Zhang[1], Junling Li[1], Yuzhe Zhang[1], Xiaohui Du[1], Kai Zhang[1], Jiaqi Wang[1]

[1]State Key Laboratory of Environmental Criteria and Risk Assessment, Chinese Research Academy of Environmental Sciences, Beijing 100012, China

Correspondence to: Jiaqi Wang (wang.jiaqi@craes.org.cn), Kai Zhang (zhangkai@craes.org.cn)

Abstract. The production mechanism of atmospheric nitrous acid (HONO), an important precursor of hydroxyl radical (OH), was still controversial. Few studies have explored the effects of particulate nitrate photolysis on HONO sources in different environment conditions across China. In this work, the photolysis rate constants of particulate nitrate for HONO production ($J_{NO_3^- - HONO}$) were determined through photochemical reaction system with $PM_{2.5}$ samples collected from five representative sites in China. We developed a method to correct and quantify the "shadowing effect" — potential light extinction within aerosol layers at heavy $PM_{2.5}$ loadings on the filters — for $J_{NO_3^- - HONO}$ measurements, which showing that elemental carbon (EC), the dominant light-absorbing component in $PM_{2.5}$, played a dominant role in it. The corrected $J_{NO_3^- - HONO}$ values varied with sampling period and location over a wide range, distributing from 1.6×10^{-6} s^{-1} to 1.96×10^{-4} s^{-1}, with a mean (± 1 SD) of $(1.71\pm2.36)\times10^{-5}$ s^{-1}. Chemical compositions, specifically nitrate loading and organic component, affected the production of HONO through particulate nitrate photolysis: high $J_{NO_3^- - HONO}$ values were generally associated with the $PM_{2.5}$ samples with high OC/NO_3^- ratio (R^2=0.86). We suggested that the parameterization equation between $J_{NO_3^- - HONO}$ and OC/NO_3^- established in this work can be used to estimate $J_{NO_3^- - HONO}$ in different aerosol chemical conditions, thus reducing the uncertainty in exploring HONO daytime sources. This study confirms that the photolysis of particulate nitrate can be a potential HONO daytime source in rural or southern urban sites, which are characterized by high proportion of organic matter in $PM_{2.5}$.

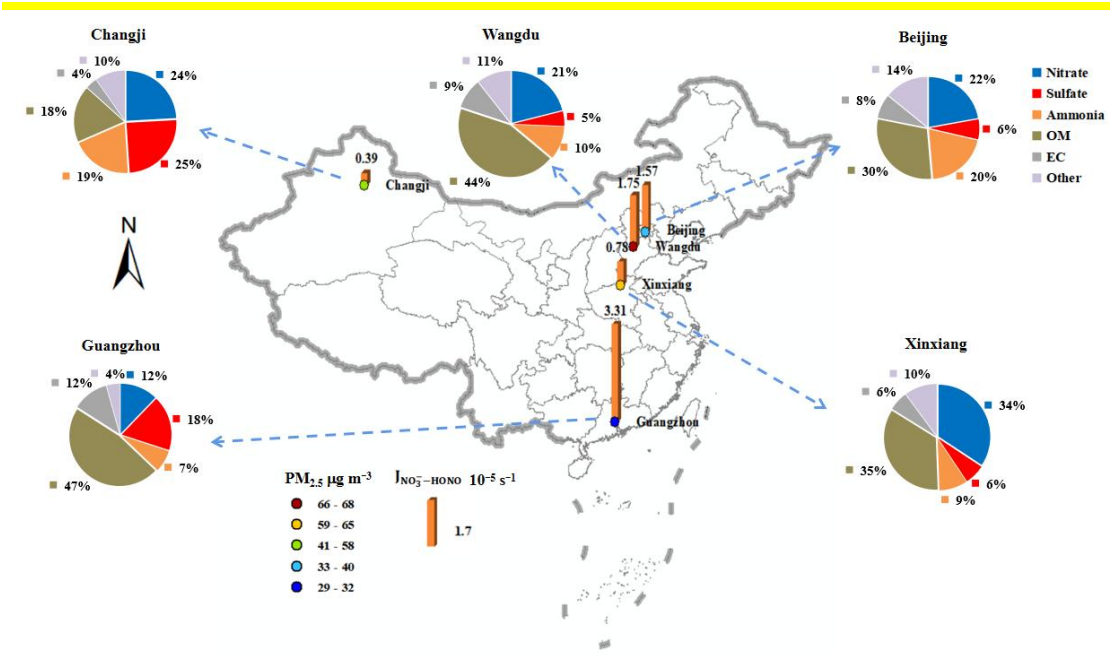
Changji
Wangdu
Beijing
Guangzhou
Xinxiang
Nitrate
Sulfate
Ammonia
OM
EC
Other
0.39
1.57
1.75
0.78
3.31
N
PM2.5 μg m−3
66 - 68
59 - 65
41 - 58
33 - 40
29 - 32
JNO3−HONO 10−5 s−1
1.7

29

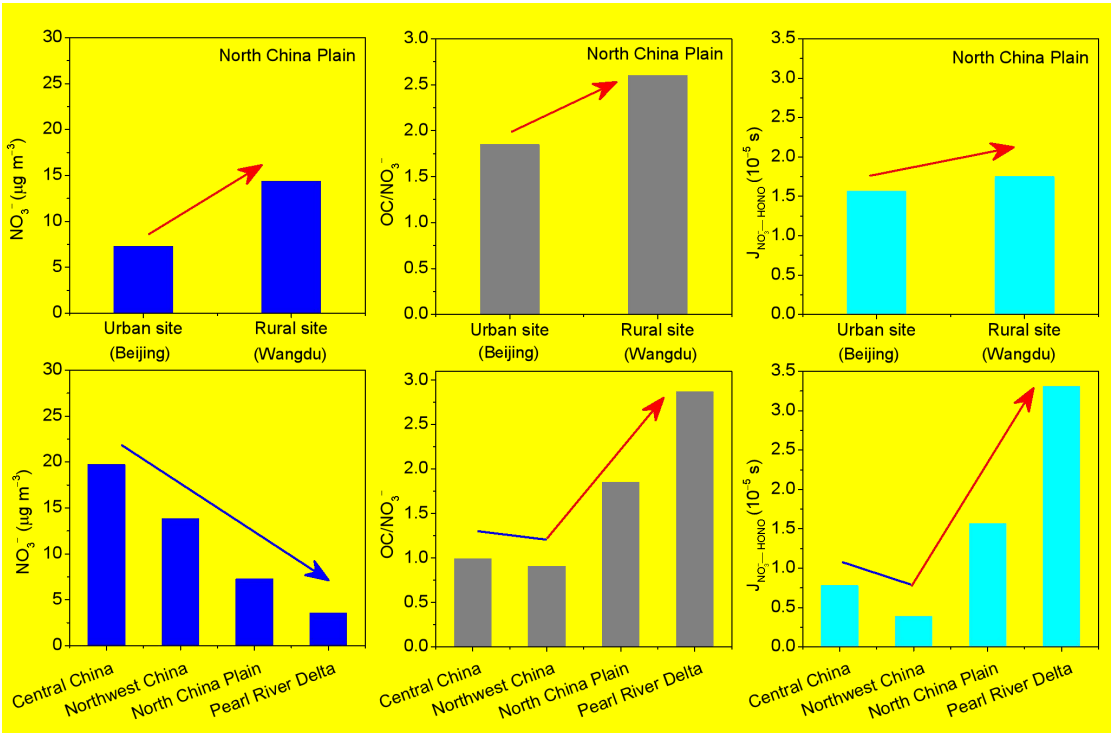
North China Plain
NO3− (μg m−3)
OC/NO3−
JNO3−HONO (10−5 s)
Urban site
(Beijing)
Rural site
(Wangdu)
Central China
Northwest China
North China Plain
Pearl River Delta

30

1 Introduction

Gaseous nitrous acid (HONO) is an important nitrogen-containing trace gas in the troposphere, which can produce hydroxyl radical (OH) through photolysis, thus stimulating the enhancement of atmospheric oxidation and the formation of secondary aerosols (Fu et al., 2019; Slater et al., 2020; Ren et al., 2003; Li et al., 2011; Su et al., 2011). In recent years, the contribution of HONO to atmospheric oxidation in heavily polluted conditions has attracted great attention (Villena et al., 2011; Fu et al., 2019; Slater et al., 2020). Even though observational research on HONO has been conducted for nearly 40 years, the understanding of HONO daytime source was still controversial (Fu et al., 2019; Wang et al., 2017; Mora Garcia et al., 2021). Numerous mechanisms have been proposed to explain the extremely high HONO concentrations at noon, including direct combustion emission (Kurtenbach et al., 2001; Liang et al., 2017; Liao et al., 2021), gas-phase reaction of NO and OH radical (Li et al., 2011; Zhang et al., 2016), heterogeneous reaction of NO_2 (Wang et al., 2017; Ammann et al., 1998; Monge et al., 2010; Stemmler et al., 2006), soil emissions (Su et al., 2011; Oswald et al., 2013; Melissa A, 2014; Kim and Or, 2019), and the photolysis of HNO_3/nitrate on aerosol or ground surface (Zhou et al., 2003; Zhou et al., 2011; Ye et al., 2016b; Ye et al., 2016a; Ye et al., 2017).

Particulate nitrate, which was conventionally considered as the ultimate oxidation product of NO_x, can rapidly photolyze and recycle NO_x or HONO back to the gas phase (Andersen et al., 2023; Handley et al., 2007; Beine et al., 2006; Ye et al., 2016a; Ye et al., 2017; Ye et al., 2016b; Gu et al., 2022b), at a rate 10 to 300 times faster than the photolysis rate of gaseous HNO_3 ($\sim 7\times10^{-7}$ s^{-1}) under typical tropical noontime conditions (Finlayson-Pitts, 2000). Recently, some field, laboratory and modeling works have proposed that photolysis of particulate nitrate can be an important in situ source of HONO in rural, suburban and urban environments (Ye et al., 2016b; Mora Garcia et al., 2021; Liu et al., 2019; Bao et al., 2018; Wang et al., 2017). Fu et al. (2019) found that the photolysis of HNO_3/nitrate in the atmosphere and deposited on surfaces was the dominant HONO source during noon and afternoon, contributing above 50 % of the simulated HONO. However, there are large discrepancies in estimating the rate constants in the atmosphere (Gen et al., 2022). In New York, Ye et al. (2017) reported that the photolysis rates of particulate nitrate in clean areas were two orders of magnitude higher than that in polluted areas, ranging from 6.2×10^{-6} to 5.0×10^{-4} s^{-1}, with a median of 8.3×10^{-5} s^{-1}. The proposed rate constants of nitrate photolysis based on the aircraft observations over South Korea ranged from 7×10^{-6}

to 2.1×10^{-5} s^{-1} (Romer et al., 2018). Shi et al. (2021) derived the rate constant (< 2×10^{-5} s^{-1}) based on chamber experiments, but found a limited role of this mechanism to HONO production. The uncertainty of HONO production rate from the photolysis of particulate nitrate can reach up to 1.4 ppbv h^{-1}, and greatly affect the accuracy of HONO source analysis (Liu et al., 2019; Lee et al., 2016; Ye et al., 2016a). The highly-varied photolysis rate constant of particulate nitrate was closely associated with environmental conditions and the aerosol chemical or physical characteristics, such as relative humidity (RH), aerosol acidity, light intensity, and coexisting components (organic components, halogen, etc.) (Gelencsér et al., 2003; Ye et al., 2016a; Bao et al., 2020; Wang et al., 2021; Reeser et al., 2013). Elucidating the mechanism and dominant factors controlling the photolysis of particulate nitrate is important to accurately estimate the HONO production rates from nitrate photolysis, thus improving estimations of HONO budgets.

In general, the photolysis rate constant of particulate nitrate was derived though photochemical experiments using bulk particle samples collected on filters (Ye et al., 2017; Bao et al., 2018). Comparing with the suspended particles in the ambient atmosphere, the collected $PM_{2.5}$ particles in the aerosol filters may present a multiple-layer structure, especially in heavy air pollution conditions (Bao et al., 2018). The light-absorbing species within $PM_{2.5}$ particles would hinder the light absorption of particulate nitrate in the lower layers of the filter sample, thus inhibiting the photolysis of particulate nitrate, which was called the "shadowing effect" (Ye et al., 2017). The shadowing effect may be negligible in clean air conditions but should be evaluated and quantified in heavy haze conditions. However, previous works generally ignored this shadowing effect.

According to previous field observations, the $PM_{2.5}$ chemical composition, especially particulate nitrate (NO_3^-), showed obvious spatial differences across China (Wang et al., 2022a, b; Wang et al., 2022c; Wang et al., 2016; Cheng et al., 2024). As one of the key industrial development areas in China, the Pearl River Delta Region (PRD) has a great number of large-scale industrial parks dominated by the chemical industry, resulting in significant VOC emissions and a large proportion of organic matter (OM) in $PM_{2.5}$. In the North China Plain (NCP), the particulate nitrate (NO_3^-) has surpassed sulfate (SO_4^{2-}) and OM to become the dominant $PM_{2.5}$ component in recent years (Wang et al., 2022b). For now, the investigation of particulate nitrate photolysis in different atmospheric environments was limited in China, and the influence of aerosol chemical or physical characteristics on HONO production was still unclear. In this work, to shed light on the contribution of particulate nitrate photolysis to the HONO

daytime source, we examined the photolysis rate constant for HONO based on photochemical experiments with $PM_{2.5}$ samples collected from five typical sites in China. In addition, the shadowing effect due to increasing aerosol particle loading on the filters was quantified. After correcting this effect, the influence of various environmental conditions, including particulate nitrate, organic matter, and aerosol acidity, on the formation of HONO was investigated and the possible role of this photolytic process as HONO sources was also examined.

2 Method

2.1 Sampling and filter treatment

The ambient $PM_{2.5}$ was collected on Teflon or quartz filters in autumn-winter seasons in five representative sites, i.e., Beijing, Wangdu, Xinxiang, Guangzhou, and Changji, which were shown in Figure 1a and described in detail in the Supporting Information. These cities were located in the North China Plain (NCP, urban: Beijing, rural: Wangdu), Central China, Pearl River Delta Region (PRD), and Northwestern China, respectively. The sampling flow rates ranged from 16.7 to 1050 L min^{-1}, the sampling times from 9 h to 23 h, and the overall sampling volumes of air from 8 m^3 to 1450 m^3, to collect a very wide range of particulate nitrate loadings. The comparison experiments between Teflon and quartz filters have been conducted, and no significant differences in HONO production rates from particulate nitrate photolysis have been found ($T<0.01$). The sampling settings employed in Wangdu were designed to quantify the shadowing effect (Figure 1b). In Wangdu, $PM_{2.5}$ was collected at a flow rate of 16.7 L min^{-1} with four channels (A, B, C, and D). A and B channels were set for daytime(8:00−17:00) and nighttime (18:00−7:00) $PM_{2.5}$ samples, respectively, and the other two channels were for the "all-day" (including 8:00−17:00 and 18:00−7:00) $PM_{2.5}$ samples. A total of 158 effective $PM_{2.5}$ samples were obtained in this study. These aerosol filter samples were labeled and stored at −20°C in the freezer.

Fractions with given surface area from each filter sample were used to perform photochemical reaction experiments and analysis of aerosol chemical components. For each $PM_{2.5}$ sample, the fraction with given surface area was rinsed by deionized water and then sonicated for 15 min. The amounts of water-soluble ions including Na^+, NH_4^+, K^+, Mg^{2+}, Ca^{2+}, Cl^-, NO_3^-, and SO_4^{2-} were measured by ion chromatography (IC, Thermo ICS-2100). To measure the values of carbon components, including

organic carbon (OC) and elemental carbon (EC), a part (0.5024 cm^2) of each filter was detected using a thermal optical carbon analyzer (DRI model 2015). The concentration of OM was obtained by multiplying the OC concentration by a factor of 1.6 (Li et al., 2021). $PM_{2.5}$ concentration was estimated by the sum of all the water-soluble ions and carbon components. The surface concentration of $PM_{2.5}$ and its components on aerosol filters were calculated through dividing the absorbed loading with the geometric area of the aerosol filter sample (μg cm^{-2}).

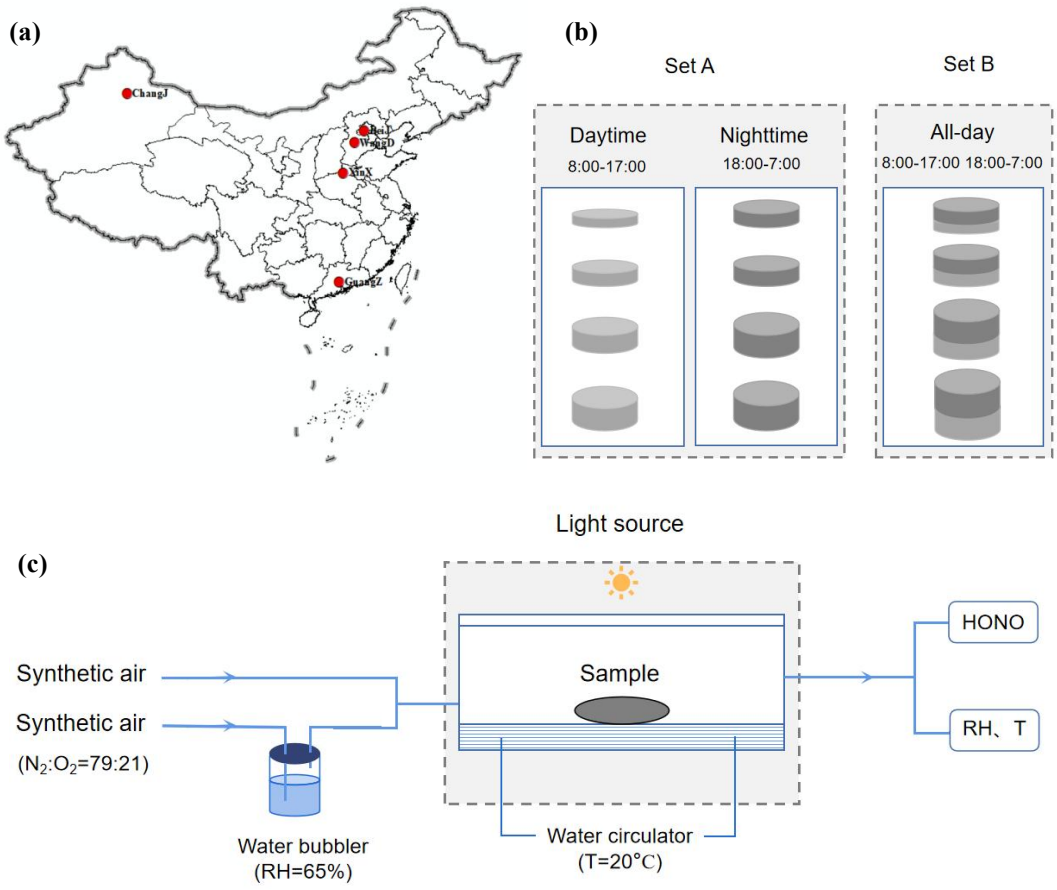

Figure 1. (a) Location map of five representative sampling sites in China, (b) the sampling settings to quantify the shadowing effect in Wangdu, and (c) a schematic diagram of the photochemical experimental setup.

2.2 Photochemical reaction system

A custom-made cylindrical quartz vessel was used as the photochemical flow reactor (Figure 1c). The diameter was 10 cm and the depth was 2.5 cm, with a cell volume of ~200 ml. A xenon lamp (300 W) was placed 20 cm above the reactor as the light source. The light was filtered by a Pyrex sleeve to remove heat-generating infrared light. The effective light intensity in the center of the flow reactor,

where aerosol samples were placed, was measured to be about 0.5 times higher (1.5 kW m^{-2} , measured by a calibrated optical power meter) than that at tropical noon on the ground (solar elevation angle θ=0°). Synthetic air, composed of ultrahigh-purity nitrogen and ultrahigh-purity oxygen mixed at a ratio of 79:21, was used as the carrier gas. The relative humidity (RH) in the air flow was adjusted through a water bubbler and monitored with an online RH sensor (Vaisala, HMT130). The aerosol filter sample was exposed to the solar simulator radiation for 20 min. The photochemical reaction experiment for each sample was repeated 2−3 times with different fractions from the same sample. The gaseous product (i.e., HONO) released during the experiment was flushed out of the reactor by the carrier gas and was detected online by a custom-built HONO analyzer, which had been applied in several measurements previously (Zhang et al., 2020b; Li et al., 2021).

2.3 HONO Production from the photolysis of particulate nitrate

The production rates (nmol h^{-1}) of HONO from particulate nitrate photolysis (P_{HONO}) were calculated from their time-integrated signals above the baselines over the period of light exposure:

$$P_{HONO} = \frac{F_g \times 60}{V_m(t_2 - t_1)} \int_{t_1}^{t_2} C_{HONO} dt \quad (1)$$

Where F_g (L min^{-1}) is the flow rate of the carrier gas, V_m (24.5 L mol^{-1}) is the molar volume of gas at 25 °C and 1 atm of pressure; t_1 and t_2 (min) are the starting and ending time of the irradiation, respectively; C_{HONO} (ppb) is the online measured concentration of HONO. With the flow rate of 2.5 L min^{-1}, the residence time in the reaction system was around ~5 s. The photolytic loss of HONO was less than 5 %, thus no correction was made in the calculation of HONO production.

The photolysis rate constant of particulate nitrate leading to HONO production ($J_{NO_3^- - HONO}$, s^{-1}) was calculated by the following equation:

$$J_{NO_3^- - HONO} = \frac{P_{HONO}}{N_{NO_3^-} \times 3600} \quad (2)$$

Where $N_{NO_3^-}$ (mol) is the amount of NO_3^- in the tested $PM_{2.5}$ sample. In principle, the photolysis rate constant should be calculated on the amount of NO_3^- that is reachable to the irradiation. However, the amount of the light-reachable NO_3^- in the $PM_{2.5}$ sample was hard to quantify. In this work, the deviation of $J_{NO_3^- - HONO}$ due to the overestimate of the amount of NO_3^- under light irradiation, which was called the shadowing effect, would be corrected in Sect. 3.1.

3 Results

3.1 Quantify the influence of the shadowing effect

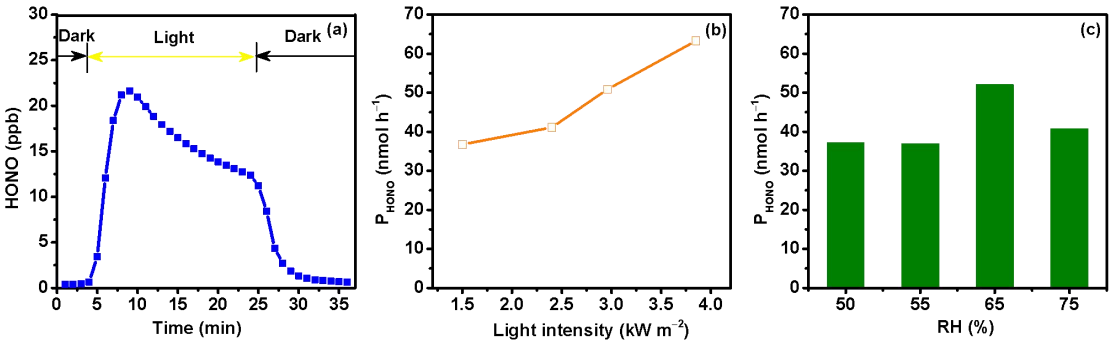

Figure 2. (a) Online measured concentrations of HONO during the light-exposure of an aerosol sample collected on June 12, 2023 in Beijing, P_{HONO} as a function of (b) light intensity (kW m^{-2}) and (c) RH (%).

HONO production within the first 20 min of irradiation during the photochemical experiment was investigated on the $PM_{2.5}$ samples collected from five typical sites in China. Figure 2a showed a typical profile of the changes in HONO concentration in the reaction system. When the light was turned on, HONO concentration in the reactor increased immediately, then leveled off and slightly decayed afterwards. After the light was turned off, the HONO generation stopped immediately and the signal nearly returned to the baseline level. Previous works have revealed that the decay of HONO generation during light exposure period was not resulted from the evaporation loss of particulate nitrate (Ye et al., 2017), but mainly related to the inhomogeneity of particulate nitrate photochemical reactivity or the consumption of reactive electron donors (Bao et al., 2018). HONO production from the photochemical reactions of particulate nitrate were significantly influenced by ambient environmental conditions (i.e., light intensity and RH). As shown in Figure 2b, with the increase of light intensity, P_{HONO} gradually increased, with P_{HONO} in 3.85 kW m^{-2} approximately twice than that in 1.50 kW m^{-2}. Previous works found that the formation of HONO was negligible at low RH (<5%), and increased at intermediate RH (15%−75%), then turned to decrease at RH > 90% (Bao et al., 2018) . Here, we found that P_{HONO} climbed to its highest when RH was around 65 % (Figure 2c). In this work, the photochemical reactions on different aerosol samples were all conducted under the same environmental condition (RH=65 %, temperature=20 °C, and light intensity=1.50 kW m^{-2}).

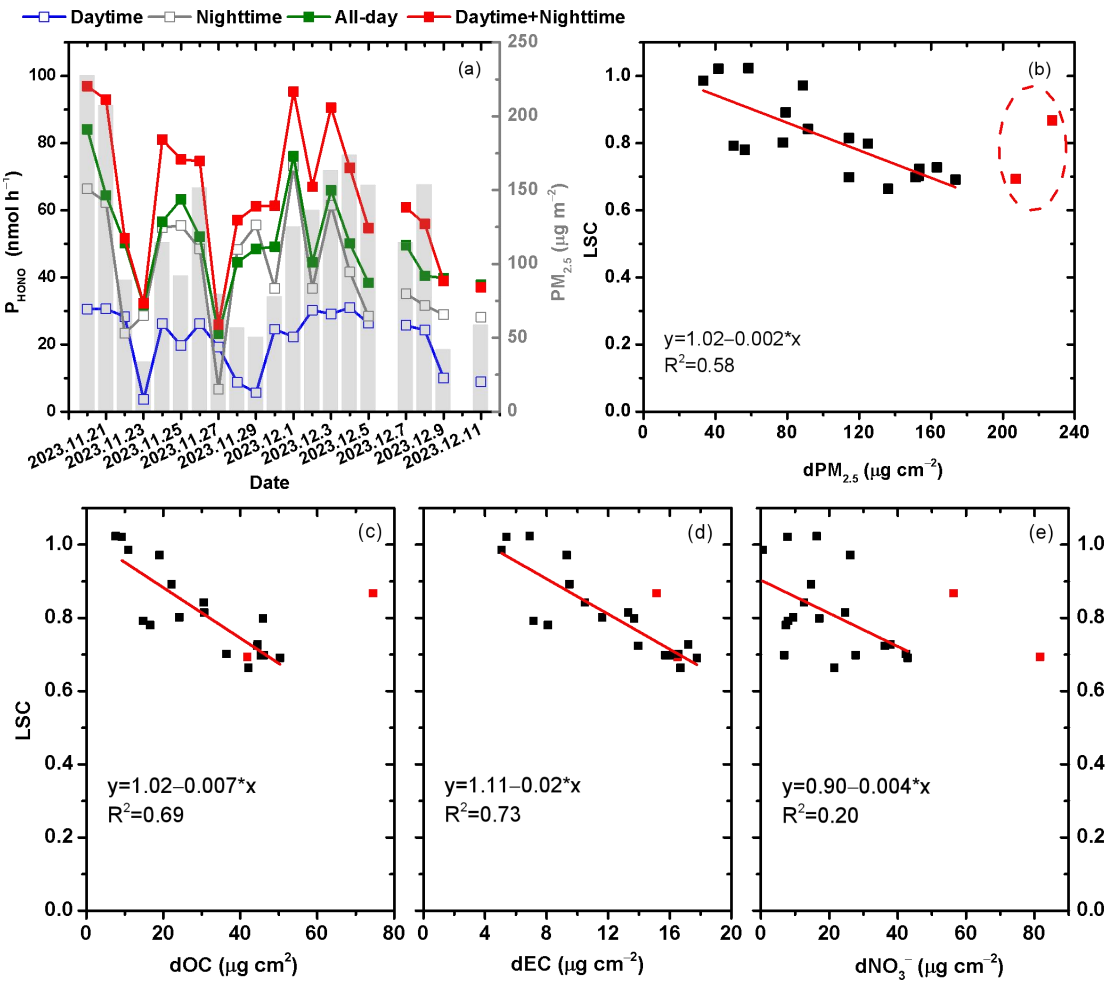

Figure 3. (a) Temporal variation of P_{HONO} for aerosol filters collected in Wangdu during daytime, nighttime and all-day from November 20, 2023 to December 11, 2023, (b)-(e) relationships between light screening coefficient (LSC) and the surface concentrations of $PM_{2.5}$ ($dPM_{2.5}$), OC (dOC), EC (dEC) and NO_3^- (dNO_3^-), respectively. The red squares represent the aerosol samples with $PM_{2.5}$ surface concentration higher than 200 μg cm^{-2}.

As expected, P_{HONO} increased with particulate nitrate loadings in different sampling locations (Figure S1), however, it's interesting to note that, P_{HONO} did not increase or somewhat decreased at very high NO_3^- loading condition. Previous works considered this may be attributed to the shadowing effect, wherein the particulate nitrate underneath the aerosol filters may receive less UV light at heavy aerosol particle loading on the filters, inhibiting the photolysis of particulate nitrate (Ye et al., 2017). Thus, the reported P_{HONO} values for the aerosol filters collected under polluted ambient conditions would be underestimated with heavy aerosol particle loading. To verify and quantify the underestimation of P_{HONO} due to the shadowing effect, we collected two sets of filters in Wangdu (set A: daytime and nighttime, set B: all-day, Figure 1b). Theoretically, the all-day one should share the same NO_3^- loading

and chemical composition as the sum of the daytime and nighttime filters, thus the sum of P_{HONO} during daytime ($P_{daytime}^{HONO}$) and nighttime ($P_{nighttime}^{HONO}$) should be equal to that during all-day ($P_{all-day}^{HONO}$) without considering the shadowing effect. A total of 20 pairs of comparative photochemical experiments were conducted, and the comparison of P_{HONO} between these two sets of filters was shown in Figure 3a. We found that the discrepancy between $P_{all-day}^{HONO}$ and $P_{daytime}^{HONO} + P_{nighttime}^{HONO}$ was widening along with the increase of surface $PM_{2.5}$ concentration. To quantify the shadowing effect, we introduced a parameter called "light screening coefficient" (LSC) to describe the decreasing efficiency of light penetrating into the particle with increasing $PM_{2.5}$ loadings:

$$P_{theory}^{HONO} = P_{daytime}^{HONO} + P_{nighttime}^{HONO} \quad (3)$$

$$LSC = P_{observed}^{HONO} / P_{corrected}^{HONO} = P_{all-day}^{HONO} / P_{theory}^{HONO} \quad (4)$$

where $P_{observed}^{HONO}$ represented the observed production rate of HONO from particulate nitrate photolysis through photochemical experiment, and $P_{corrected}^{HONO}$ represented the corrected value of P_{HONO} after quantifying the shadowing effect. As shown in Figure 3b, when $PM_{2.5}$ surface concentration ($dPM_{2.5}$) was low, LSC was almost equal to 1, indicating that the shadowing effect was negligible. With the increase of $PM_{2.5}$ loading, the value of LSC declined to lower than 65 %. In general, significant negative correlation exited between LSC and $dPM_{2.5}$, except when $dPM_{2.5}$ was higher than 200 μg cm^{-2} (Figure 3b). In this experiment, we assumed that the daytime and nighttime $PM_{2.5}$ samples were both single-layered. However, with the increase of air pollution, these filters in each pair of comparative experiments may already have exhibited the shadowing effect, thus the sum of $P_{daytime}^{HONO}$ and $P_{nighttime}^{HONO}$ would be underestimated. Therefore, when quantifying the shadowing effect, the LSC data with $PM_{2.5}$ loading higher than 200 μg cm^{-2} was excluded. Correlations between LSC and the surface concentrations of $PM_{2.5}$ major chemical components, such as EC (dEC), OC (dOC), and NO_3^- (dNO_3^-), were conducted (Figure 3c-e). Significant correlation was found between LSC and carbonaceous component, especially EC (R^2=0.73), which was one of the most important light absorbing species in $PM_{2.5}$, indicating that the shadowing effect was mainly related to the light absorption components in $PM_{2.5}$. The relationship between LSC and dEC was established as following:

$$dEC > 5.5\ \mu g\ m^{-2}: LSC = 1.11 - 0.02 \times dEC$$

$$dEC \leq 5.5\ \mu g\ m^{-2}: LSC = 1 \quad (5)$$

when $dEC \leq 5.5\ \mu g\ m^{-2}$, the shadowing effect can be ignored; when $dEC > 5.5\ \mu g\ m^{-2}$, P_{HONO} can be corrected by the observed P_{HONO} and LSC, which was estimated using this fitting equation with dEC.

Previous works found that the heavy loads of carbonaceous particles can turn these filters into dark brown colors. The UV light was unlikely to transmit efficiently through the dark layer to the particulate nitrate underneath, thus inhibiting the generation of HONO from the photolysis of particulate nitrate (Ye et al., 2017). In consideration of the potential shadowing effect for the daytime and nighttime filters in each pair of comparative experiments, the $P^{HONO}_{daytime}$ and $P^{HONO}_{nighttime}$ observed would be underestimated, and the uncertainty of LSC should be considered at high $PM_{2.5}$ loadings. To evaluate this uncertainty, the observed $P^{HONO}_{daytime}$ and $P^{HONO}_{nighttime}$ values were recalculated and corrected to the theoretical single-layered condition based on Eq. (4) and (5). As shown in Figure S2, with the increase of $PM_{2.5}$ surface concentration, the deviations between LSC and the corrected one have enlarged. However, it's noted that the deviation was still lower than 20 % when $PM_{2.5}$ surface concentration was around 200 μg cm^{-2}. For example, for the aerosol sample collected in December 4, 2023, in Wangdu, the $PM_{2.5}$ surface concentration was 173.57 μg cm^{-2}, and the deviation was 15.74 %, which was acceptable in this work.

3.2 Spatial distribution and temporal variation of HONO production from particulate nitrate photolysis

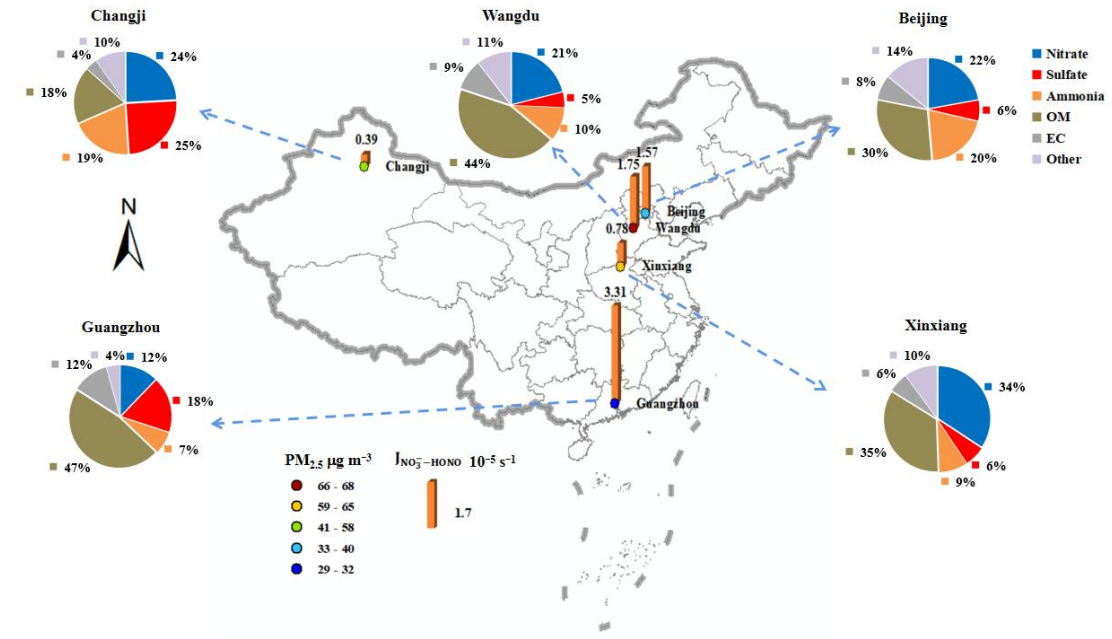

Figure 4. Spatial distribution of the average ($J_{NO_3^- - HONO}$), $PM_{2.5}$ loading, and chemical composition of the aerosol filters collected from five representative cities in China during the observation period.

There were 158 filter samples collected from five representative cities in China, and the averaged concentrations of $PM_{2.5}$ and its chemical composition of these filters showed significant spatial

characteristics as shown in Figure 4. During the sampling period, OM was the most abundant species in $PM_{2.5}$ over most regions, except in the northwestern city (Changji), and NO_3^- was the dominant inorganic component in the NCP (Beijing and Wangdu) and Central China (Xinxiang), while SO_4^{2-} showed the highest contribution in the PRD (Guangzhou) and Northwestern China (Changji). The values of $J_{NO_3^- - HONO}$ on these $PM_{2.5}$ samples were calculated by Eq. (2) with the P_{HONO} corrected by Eq. (4) and (5), and summarized in Figure 4 and Table 1. The corrected $J_{NO_3^- - HONO}$, median and mean (± one standard deviation), were 1.55×10^{-5} s^{-1} and 1.57 (±2.14) $\times10^{-5}$ s^{-1} in Beijing, 1.68×10^{-5} s^{-1} and 1.75 (±2.83) $\times10^{-5}$ s^{-1} in Wangdu, 0.69×10^{-5} s^{-1} and 0.78 (±0.48) $\times10^{-5}$ s^{-1} in Xinxiang, 3.04×10^{-5} s^{-1} and 3.31 (±1.15) $\times10^{-5}$ s^{-1} in Guangzhou, and 0.38×10^{-5} s^{-1} and 0.39 (±0.25) $\times10^{-5}$ s^{-1} in Changji, respectively. The maximum $J_{NO_3^- - HONO}$ in these cities ranged from 0.91×10^{-5} s^{-1} in Changji to 1.96×10^{-4} s^{-1} in Wangdu. These values were in the comparable range to those previously reported for aerosol samples, such as 1.22×10^{-5} s^{-1}~ 4.84×10^{-4} s^{-1} in China by Bao et al. (2018) (RH = 60%, temperature = 25°C, irradiation time=15 min) and 6.2×10^{-6} to 5.0×10^{-4} s^{-1} (the sum of HONO and NOx production, with an average HONO/NOx production ratio of ~2) in US by Ye et al. (2017) (RH = 50%, temperature = 20(±1)°C, irradiation time=10 min). It's interesting to note that the average $J_{NO_3^- - HONO}$ was the highest in Guangzhou, which was characterized with the lowest $PM_{2.5}$ and NO_3^- concentration among these cities. As for other cities with high $PM_{2.5}$ concentrations, such as Changji and Xinxiang, the corrected $J_{NO_3^- - HONO}$ was comparatively lower. According to the National Ambient Air Quality Standard of China (GB3095-2012), the daily $PM_{2.5}$ averages in Guangzhou can meet the Level II standard of 75 μg m^{-3}, while exceeding the level I standard (35 μg m^{-3}). Here, we defined $PM_{2.5}$ polluted days with daily mean $PM_{2.5}$ exceeding 35 μg m^{-3}. As shown in Figure 5, the distribution of the corrected $J_{NO_3^- - HONO}$ values in clean days were generally more dispersed and higher than those in polluted days, except in Guangzhou. The average value of $J_{NO_3^- - HONO}$ in Guangzhou during air polluted conditions was slightly higher than that in clean conditions, besides much higher than the values in other cities. Because the influence of the shadowing effect has been corrected to some degree, these spatial and temporal change characteristics of $J_{NO_3^- - HONO}$ in this work should be mainly related to the varied chemical and physical properties of $PM_{2.5}$ samples collected from different atmospheric environments.

Table 1. The concentrations of $PM_{2.5}$, NO_3^-, and OC, OC/NO_3^-, corrected $J_{NO_3^- - HONO}$, and S_{HONO} in five representative cities in China under different air conditions during the sampling period.

Site	Air condition	$PM_{2.5}$ ($\mu g\ m^{-3}$)	NO_3^- ($\mu g\ m^{-3}$)	OC ($\mu g\ m^{-3}$)	OC/NO_3^-	Corrected $J_{NO_3^-\text{-HONO}}$ ($10^{-5}\ s^{-1}$) [a]	S_{HONO} (10^{-5} mol $h^{-1}\ m^{-2}$) [b]	S_{HONO} (ppbv h^{-1}) [c]
Beijing	Clean	19.71±8.65	3.15±2.34	3.89±2.13	2.25±3.03	2.01±2.44	0.15±0.07	0.03±0.02
	Polluted	72.56±23.78	19.71±10.72	12.62±2.18	0.87±0.62	0.61±0.30	0.38±0.11	0.09±0.02
	Whole-Min	4.32	0.08	1.07	0.32	0.21	0.04	0.01
	Whole-Max	102.64	32.90	15.95	12.82	11.06	0.57	0.13
	Whole-Mean	32.92	7.29	6.07	1.85	1.57	0.22	0.05
Changji	Clean	20.39±6.00	3.05±1.75	3.61±1.08	1.66±1.11	0.65±0.18	0.07±0.03	0.02±0.01
	Polluted	80.49±39.54	20.59±4.74	8.35±2.97	0.44±0.08	0.21±0.03	0.16±0.04	0.04±0.01
	Whole-Min	14.45	0.88	2.69	0.28	0.16	0.03[d]	0.01[d]
	Whole-Max	169.35	28.28	14.34	3.65	0.91	0.22	0.05
	Whole-Mean	57.37	13.84	6.53	0.91	0.39	0.13	0.03
Guangzhou	Clean	25.62±6.08	3.29±1.68	6.89±2.21	2.72±1.79	3.25±1.28	0.36±0.15	0.08±0.03
	Polluted	40.32±2.23	4.38±1.30	13.82±1.34	3.35±0.86	3.53±0.61	0.59±0.15	0.13±0.03
	Whole-Min	14.77	0.85	3.67	0.82	1.37	0.17	0.04
	Whole-Max	42.74	6.63	15.62	8.05	5.83	0.75	0.17
	Whole-Mean	29.12	3.55	8.54	2.87	3.31	0.41	0.09
Wangdu	Clean	22.16±7.66	3.29±2.59	5.36±2.38	4.79±6.46	3.80±5.10	0.20±0.09	0.04±0.02
	Polluted	83.53±30.47	18.06±12.48	23.23±9.62	1.88±1.67	1.09±0.87	0.50±0.15	0.11±0.03
	Whole-Min	10.67	0.24	2.72	0.22	0.23	0.06	0.01
	Whole-Max	173.45	60.28	63.07	22.06	19.60	0.88[e]	0.20[e]
	Whole-Mean	68.38	14.41	18.82	2.60	1.75	0.42	0.10
Xinxiang	Clean	23.53±5.45	4.35±1.41	5.69±2.46	1.37±0.61	1.28±0.49	0.21±0.07	0.05±0.02
	Polluted	68.98±33.43	24.87±21.5	14.63±4.41	0.87±0.45	0.62±0.35	0.40±0.12	0.09±0.03
	Whole-Min	18.32	2.37	2.33	0.30	0.19	0.09	0.02
	Whole-Max	143.10	73.47	22.06	2.02	1.96	0.59	0.13
	Whole-Mean	57.62	19.74	12.40	0.99	0.78	0.35	0.08

[a] represented the photolysis rate constant of particulate nitrate leading to HONO production after considering the influence of the shadowing effect. [b, c] represented the noontime source strength of HONO through the photolysis of particulate nitrate with the units of 10^{-5} mol h^{-1} m^{-2} and ppbv h^{-1}, respectively. [d, e] represented the minimum and maximum values of S_{HONO} during the observation period.

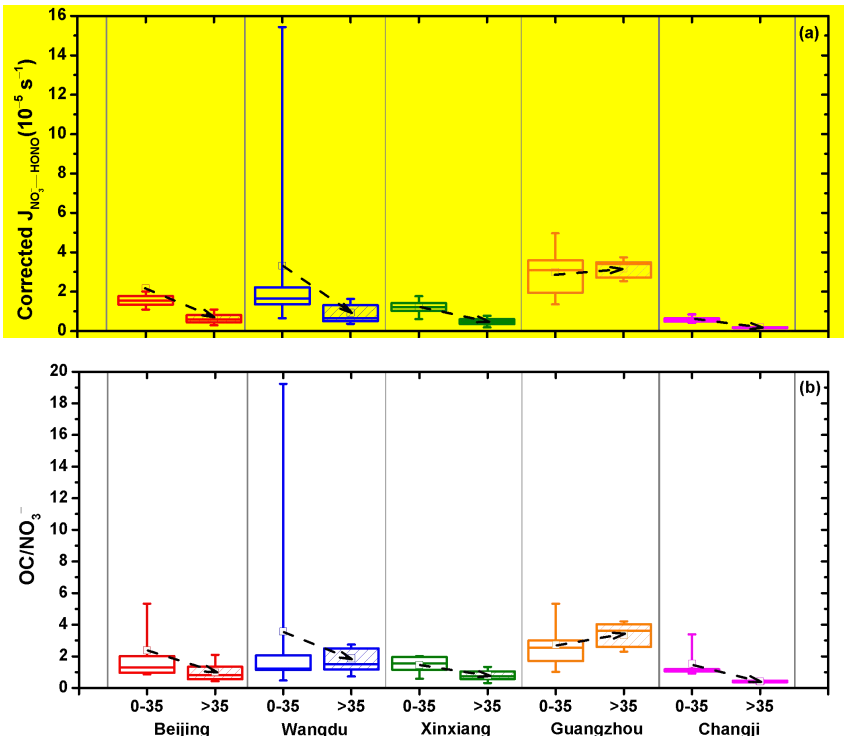

Figure 5. (a) Average corrected $J_{NO_3^- - HONO}$, and (b) the ratio of OC to NO_3^- under different air conditions in five representative cities. The box represents the 25th to 75th percentiles, the horizon line represents the median, the hollow square represents the mean, and the 10th and the 90th percentiles are the bottom and top whiskers, respectively.

3.3 Dominant factors controlling $J_{NO_3^- - HONO}$

3.3.1 Particulate nitrate

As shown in Table 1, the corrected $J_{NO_3^- - HONO}$ values varied with sampling periods and locations over a wide range, distributing from 0.16×10^{-5} s^{-1} for the aerosol sample collected in Changji with $PM_{2.5}$ higher than 90 μg m^{-3}, to 19.60×10^{-5} s^{-1} for the aerosol sample collected in Wangdu with $PM_{2.5}$ lower than 25 μg m^{-3}. Several factors may contribute to the discrepancy of $J_{NO_3^- - HONO}$ in these different aerosol samples, such as particulate nitrate, organic matter, and aerosol acidity.

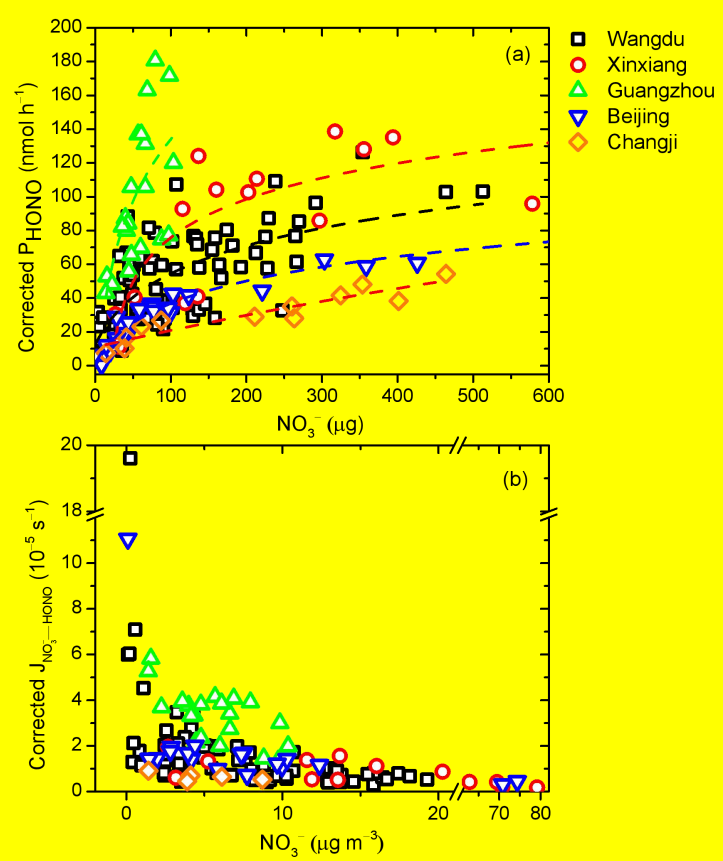

298

299 **Figure 6.** Relationships between (a) corrected P_{HONO} and particulate nitrate loading, and (b) corrected
300 $J_{NO_3^-HONO}$ and particulate nitrate concentration in different sampling locations. The dash lines in (a)
301 were the best fits to the data for the fitting equation: the aerosol samples in Guangzhou (a=4.30, b=0.06,
302 c=1 × 10^{-6}, R^2= 0.42), Wangdu (a=2.54, b=0.11, c=1 × 10^{-6}, R^2=0.50), Beijing (a=1.51, b=0.06,
303 c=1×10^{-6}, R^2=0.91), Xinxiang (a=2.28, b=0.06, c=1×10^{-6}, R^2=0.47), and Changji (a=0.58, b=0.04,
304 c=1×10^{-6}, R^2=0.86).

305 As shown in Figure 6, after considering the shadowing effect, the corrected P_{HONO} generally
306 increased along with the increased amount of particulate nitrate (pNO_3^-, μg), but still gradually slowed
307 down at high particulate nitrate loading, resulting in a rapid decrease in $J_{NO_3^-HONO}$. For example, when
308 NO_3^- concentration was at low level (around 0.5 μg m^{-3}) in Wangdu, the value of corrected $J_{NO_3^-HONO}$
309 was about 30 times higher than that at high NO_3^- concentration (around 20 μg m^{-3}). Previous works
310 found that the particulate nitrate was associated with matrix components in aerosol samples, and the
311 photolysis reactivity of particulate nitrate was closely associated with the surface catalysis effect (Ye et
312 al., 2017). In such a mechanism, the interaction between particulate nitrate and the substrate can distort
313 the molecular structure of nitrate and increase the absorption cross-section. The increases of P_{HONO} with
314 pNO_3^- exposed to the light radiation can be fitted by a logarithm curve under different

environment: $P_{HONO} = \frac{a}{b}\ln(1 + b(pNO_3^-)) + c(pNO_3^-)$ (Ye et al., 2017; Ye et al., 2019). Based on this fitting equation, the corrected P_{HONO} as a function of pNO_3^- was showed in Figure 6a. Interestingly, these relationships under different sampling locations showed distinct upward trends. Ye et al. (2019) found that this ratio of a to b was related to the catalysis power of surface reactive sites and the organic matters in the matrix. The much higher ratio of a (4.30) to b (0.06) values fitted for Guangzhou than those for other cities, especially Changji (a=0.58, b=0.04), suggested extra catalytic power of organic components in addition to the surface reactive site on particulate nitrate. The large deviation of the ratio of a to b among these cities indicated the limitation of predicting P_{HONO} only based on the relationship with particulate nitrate in different atmospheric environments, and other varied aerosol chemical and physical conditions should be considered as well.

3.3.2 Organic matter

Organic matter was ubiquitous in the atmosphere and contributed significantly to the total aerosol mass. The selectivity of organic matter that coexisted in the aerosols was very important for the production of HONO from the photolysis of particulate nitrate (Bao et al., 2018; Ye et al., 2016a; Svoboda et al., 2013; Reeser et al., 2013; Stemmler et al., 2006; Yang et al., 2018; Beine et al., 2006; Wang et al., 2021). As shown in Figure 7a, corrected P_{HONO} generally increased as the amount of OC in aerosol samples (pOC, μg) went up, while these positive correlations between P_{HONO} and pOC shown may be due to the moderate correlation between pNO_3^- and pOC (R^2=0.39, Figure S3). To eliminate the contribution from particulate nitrate, the dependence of $J_{NO_3^- - HONO}$ on the ratio of OC to NO_3^- (OC/NO_3^-) was examined:

Corrected $J_{NO_3^- - HONO}$=0.74×(OC/NO_3^-)+0.08 (6)

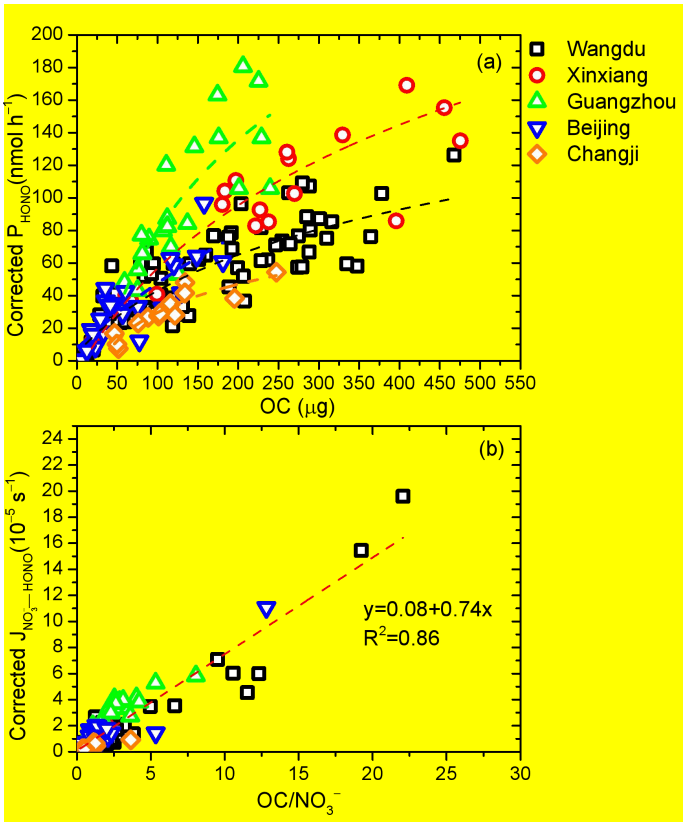

336

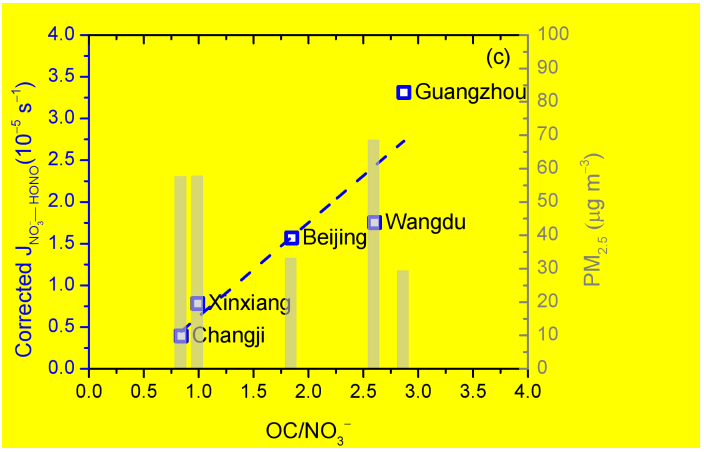

337

338 **Figure 7.** Relationship between (a) corrected P_{HONO} and OC loadings, (b) corrected $J_{NO_3^-–HONO}$ and
339 OC/NO_3^-, and (c) average corrected $J_{NO_3^-–HONO}$, $PM_{2.5}$, and OC/NO_3^- during the sampling period in
340 five representative cities.

341 As shown in Figure 7b, significant linear correlation between corrected $J_{NO_3^-–HONO}$ and OC/NO_3^-
342 was found, with an R^2 of 0.86. In general, high corrected $J_{NO_3^-–HONO}$ values were mostly associated
343 with high OC/NO_3^- ratios for aerosol samples collected in the clean areas, such as Guangzhou, where
344 the averaged $PM_{2.5}$ level was the lowest (Figure 7c). Low corrected $J_{NO_3^-–HONO}$ values were mostly
345 associated with low OC/NO_3^- ratio. Generally, cities with higher $PM_{2.5}$ levels have lower OC/NO_3^-
346 ratios, such as Changji and Xinxiang, however, there was an exception—Wangdu, a rural site in the

North China Plain, where the $PM_{2.5}$ was high but dominated by OM mainly due to local residential coal combustion (Liu et al., 2016; Li et al., 2024; Liu et al., 2017). As shown in Figure 5b, the OC/NO_3^- ratio in clean days was generally higher than that in polluted conditions. Interestingly, different from other cities, the OC/NO_3^- ratio in Guangzhou increased at polluted conditions, which was consistent with the correspondingly higher corrected $J_{NO_3^- - HONO}$ value. Guangzhou was located in the PRD region, and was characterized by large fractions of OM in $PM_{2.5}$ due to large emission of VOCs from numerous manufacturing industries and transport-related sources (Zheng et al., 2009), and the water-soluble organic carbon (WSOC) was the dominated component in the organic aerosols (WSOC/OC=0.63) (Chang et al., 2019). It's reported that organic compounds on the surface may act as photosensitizers in the photolysis of particulate nitrate (Gen et al., 2022; Handley et al., 2007; Cao et al., 2022; Wang et al., 2021). The association of particulate nitrate with organic matter may distort its molecular structure and enhance the absorption cross section, resulting in significantly enhancement in the photochemical production of HONO. The organic matter can also become hydrogen donors, and directly transfer hydrogen from organic H-donors to NO_2 to form HONO (Gen et al., 2022). Therefore, we suggested that the gradually increasing role of organic matter in $PM_{2.5}$ in China should be of great concern.

3.3.3 Other factors

The acidic proton may play an important role in the photochemical production of HONO and affect the release of photolysis products (Bao et al., 2018; Scharko et al., 2014). Scharko et al. (2014) found that gaseous HONO production from nitrate photolysis was the highest at the lowest aerosol acidity (pH, ~2) and decreased with pH, and reached almost zero at pH higher than 4. In this work, the estimated pH of these aerosol samples was in the range of 1.83−3.46 (the Extended Aerosol Inorganic Model, E-AIM (Shi et al., 2021; Wexler and Clegg, 2002; Clegg et al., 1998)) with detailed information provided in the Supporting Information. As shown in Figure S4, however, the correlation between pH and $J_{NO_3^- - HONO}$ was weak, which indicated that pH was an important factor, but not the key one driving the spatial differences of $J_{NO_3^- - HONO}$ in this work. Noting that halide ions, such as chlorine (Cl^-), may lead to enhancement of surface nitrate anion and promote nitrate photolysis (Gen et al., 2022; Zhang et al., 2020a), we also plotted $J_{NO_3^- - HONO}$ against the molar ratio of Cl^- to NO_3^- (Cl^-/NO_3^-) in Figure 8a. Even though Guangzhou was a southern coastal city, the sampling site in this

work was far away from the South China Sea (>50 km). Besides, during the observation period, the aerosol collected in Guangzhou was more representative of inland aerosol instead of marine aerosol, with the air parcel usually coming from inland directions (Figure 8b) and the ratio of Cl^- to NO_3^- (0.02) much lower than that in fresh sea spray aerosol (>1.0) (Xiao et al., 2017; Pipalatkar et al., 2014; Atzei et al., 2019; Wang et al., 2019). Therefore, we suggested that the halide ions were not the determining factor for the high $J_{NO_3^- - HONO}$ value in Guangzhou, and the exact role of halide ions in HONO formation through the photolysis of particulate nitrate required further investigation.

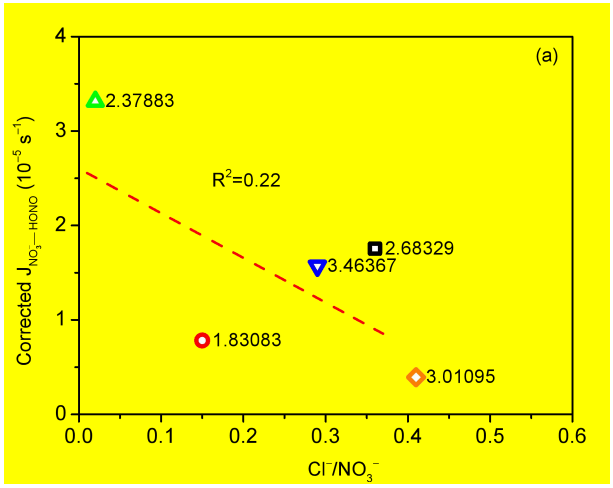

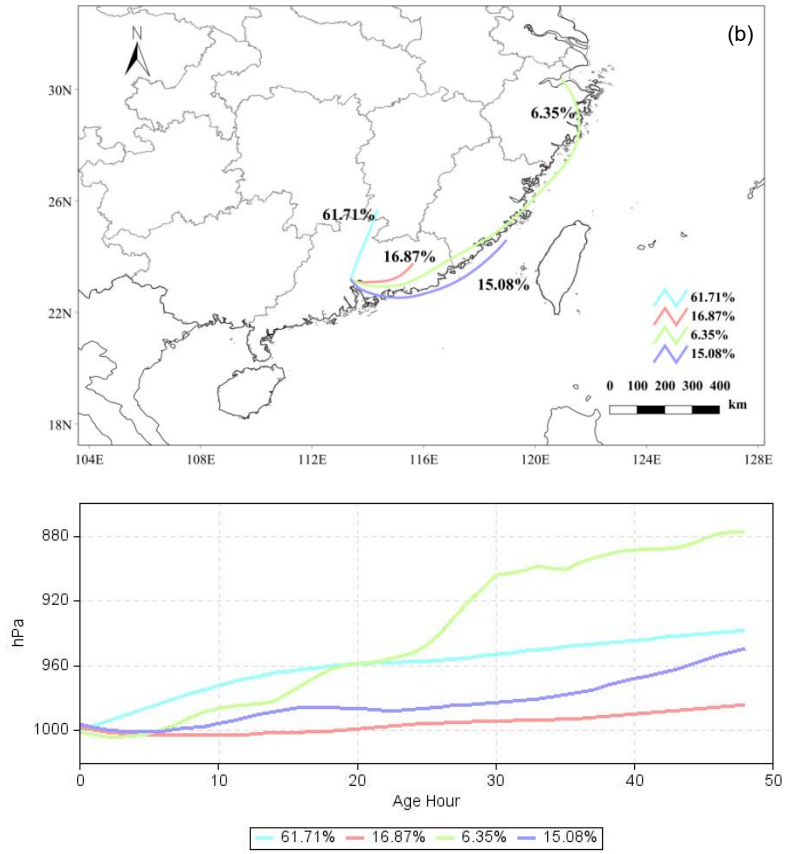

Figure 8. (a) Relationship between the average corrected $J_{NO_3^- - HONO}$ and Cl^-/NO_3^- under different

sampling locations, and (b) the back trajectory cluster analysis in Guangzhou during the sampling period.

3.4 Environmental implication

The determined $J_{NO_3^- - HONO}$ was closely associated with the aerosol chemical and physical characteristics, especially the coexisted organic components, and distributed around the curve as expressed by Eq. (6). It's the first effort to explore the photolysis of particulate nitrate in aerosol samples collected from different typical regions of China. The enhanced formation of HONO from the photolysis of particulate nitrate can contribute significantly to the atmospheric oxidation capacity. To assess the photolysis of particulate nitrate as a HONO daytime source, the noontime source strength of HONO (S_{HONO}) through this mechanism in the air column within the planetary boundary layer can be calculated by the following equation (Ye et al., 2017):

$$S_{HONO}\ (10^{-5}\ mol\ h^{-1}m^{-2}) = 0.67 \times NO_3^-(\mu mol\ m^{-3}) \times 10^{-6} \times J_{NO_3^- - HONO} \times BLH \times 3600 \quad (7)$$

or

$$S_{HONO}\ (ppbv\ h^{-1}) = 0.67 \times NO_3^-(ppbv) \times J_{NO_3^- - HONO} \times 3600 \quad (8)$$

where BLH means the boundary mixing height (m). Here, we assumed a typical BLH of 1000 m. Based on the daily measured NO_3^- and corrected $J_{NO_3^- - HONO}$ value in each city, the S_{HONO} derived from Eq. (7) or (8) during the observation period was showed in Table 1. It was found that, even though the $J_{NO_3^- - HONO}$ in polluted days was much lower than that in clean days, due to the apparent higher NO_3^- concentration, the corresponding S_{HONO} was about twice the average in clean days. The calculated S_{HONO} ranged from 0.03×10^{-5} mol h^{-1} m^{-2} to 0.88×10^{-5} mol h^{-1} m^{-2} (0.01 ppbv h^{-1}–0.2 ppbv h^{-1}), with the mean value of 0.36×10^{-5} mol $h^{-1}m^{-2}$ (0.08 ppbv h^{-1}), which was comparable or higher than other HONO sources (Bhattarai et al., 2019; Wang et al., 2023b; Ye et al., 2017). For example, the soil HONO emission flux was measured in the range of 1.81×10^{-6} mol h^{-1} m^{-2}–4.55×10^{-6} mol h^{-1} m^{-2} in the soil without suffering nitrogen fertilizer (Bhattarai et al., 2019). The mean value of S_{HONO} during the observation period was the highest in Wangdu (0.42×10^{-5} mol $h^{-1}m^{-2}$, 0.10 ppbv h^{-1}) and Guangzhou (0.41×10^{-5} mol $h^{-1}m^{-2}$, 0.09 ppbv h^{-1}), followed by Xinxiang (0.35×10^{-5} mol $h^{-1}m^{-2}$, 0.08 ppbv h^{-1}), Beijing (0.22×10^{-5} mol $h^{-1}m^{-2}$, 0.05 ppbv h^{-1}), and Changji (0.13×10^{-5} mol $h^{-1}m^{-2}$, 0.03 ppbv h^{-1}). Even though the $PM_{2.5}$ and NO_3^- concentration was the lowest in Guangzhou, the S_{HONO} was much higher than other cities with air pollution. It should be noted that the S_{HONO} calculated with the

daily changed NO_3^- and $J_{NO_3^- - HONO}$ value in this work was much lower than the value reported by Bao et al. (2018) (0.78 ppbv h^{-1}), which applied the average NO_3^- (6.64 μg m^{-3}, 2.62 ppbv) and the $J_{NO_3^- - HONO}$ range (1.22×10^{-5} s^{-1}–4.84×10^{-4} s^{-1}) to simulate S_{HONO} (0.12 ppbv h^{-1}–4.57 ppbv h^{-1}). Other works, such as Fu et al. (2019) and Gu et al. (2022a), applied the mean value of $J_{NO_3^- - HONO}$ (8.3×10^{-5} s^{-1}) and the observed NO_3^- concentration to calculate S_{HONO}. However, due to the significant decrease of $J_{NO_3^- - HONO}$ along with the increase of NO_3^-, the S_{HONO} calculated with mean NO_3^- or $J_{NO_3^- - HONO}$ will be largely overestimated, thus directly influencing the identification of HONO sources. For example, $J_{NO_3^- - HONO}$ was the highest in Wangdu in November 23, 2023 with the value of 19.6×10^{-5} s^{-1}, while the corresponding NO_3^- concentration was low (0.39 μg m^{-3}). If applying the average NO_3^- concentration (12.53 μg m^{-3}, equivalent to 4.53 ppbv) and the maximum $J_{NO_3^- - HONO}$ value, the determined S_{HONO} value would be 9.56×10^{-5} mol h^{-1} m^{-2} (2.14 ppbv h^{-1}), which was about 30 times higher than the actual result (0.07 ppbv h^{-1}). Therefore, we suggested to estimate S_{HONO} with the observed concentration of NO_3^- and the $J_{NO_3^- - HONO}$ value derived from the parameterization equation with OC/NO_3^-, thereby reducing the large uncertainties and improving estimations of HONO budget.

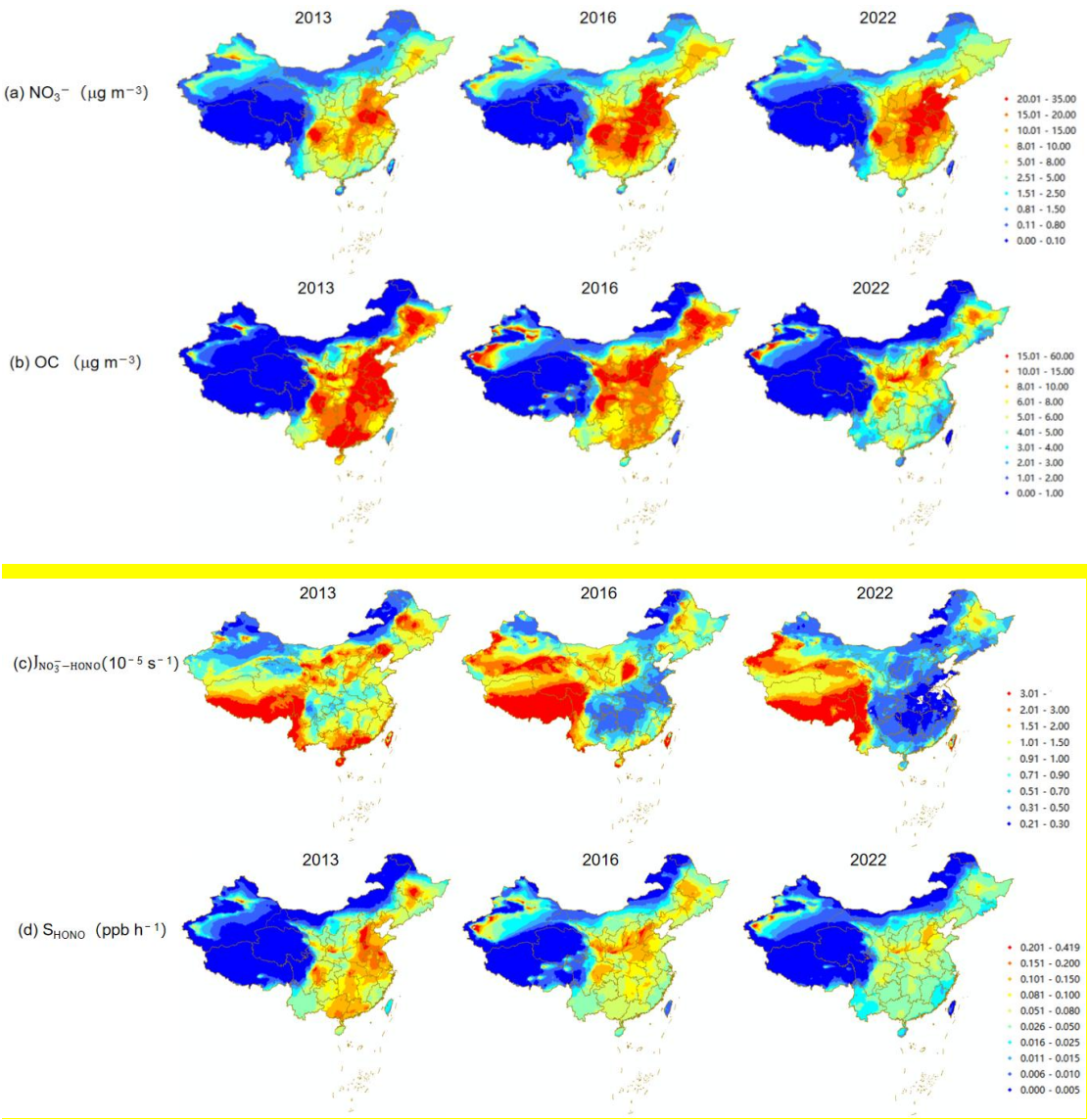

Figure 9. Spatial distributions of the daily average (a) NO_3^-, (b) OC, (c) $J_{NO_3^- - HONO}$, and (d) S_{HONO} from November 15 to December 15 in the year of 2013, 2016, and 2022 in China. The daily average concentrations of NO_3^- and OC were extracted from the Chinese high resolution $PM_{2.5}$ Component simulation concentration dataset (Kong, et al., 2024). The $J_{NO_3^- - HONO}$ and S_{HONO} estimated in this work were derived under the same environmental conditions (RH=65 %, temperature=20 °C, and light intensity=150 kW m^{-2}), thus were more representative of the potential of HONO production rather than the actual value in the real ambient environment.

On the basis of the daily average concentrations of NO_3^- and OC extracted from the Chinese high resolution $PM_{2.5}$ Component simulation concentration dataset (CAQRA-aerosol, https://www.capdatabase.cn, 15 km×15 km) (Kong, et al., 2024), the $J_{NO_3^- - HONO}$ and S_{HONO} can be estimated by Eq. (6) and (8), respectively. As shown in Figure 9, significant spatio-temporal change

characteristics of NO_3^-, OC, $J_{NO_3^-\text{-HONO}}$ and S_{HONO} were demonstrated in autumn-winter seasons from 2013 to 2022 in China. The high $J_{NO_3^-\text{-HONO}}$ were concentrated in the 'clean' environments (e.g., Tibetan Plateau area, South Xinjiang Basin, Yunnan-Guizhou plateaus, and Sichuan basins) and followed by those air polluted regions (e.g., NCP, Fenhe-Weihe Basin, Northeastern China, and PRD). From 2013 to 2022, with OC decreasing significantly, while NO_3^- keeping stable or even increasing, $J_{NO_3^-\text{-HONO}}$ showed a downward trend in most regions. Although the $J_{NO_3^-\text{-HONO}}$ in polluted regions was comparatively lower than that in 'clean' environments, the higher values of S_{HONO} were mostly distributed in these polluted regions resulting from the much higher NO_3^- concentration. However, it should be noted that the photolysis of particulate nitrate contributed only a small fraction to the needed daytime HONO source in these polluted regions, such as 1.26−3. 82 ppbv h^{-1} in the cities in the North China Plain (Hou et al., 2016; Wang et al., 2017; Lian et al., 2022; Li et al., 2018), 0.75 ppbv h^{-1} in the Western China (Huang et al., 2017), and 0.77−4.90 ppbv h^{-1} in Southern China (Li et al., 2012; Su et al., 2008). We noted that uncertainties still exist in our simulations. Given the paucity of filed measurements of HONO production from aerosol samples in 'clean' environments, the deviation of $J_{NO_3^-\text{-HONO}}$ derived from the parametrization in this work may be large in these regions. Additionally, the concentrations of NO_3^- and OC extracted from the CAQRA-aerosol in 'clean' environments were around the mean deviation level. Therefore, more field observations and simulation experiments should be taken in these 'clean' regions in the future, to enrich and improve the parametric equations of $J_{NO_3^-\text{-HONO}}$, and further evaluate the contribution of nitrate photolysis to the formation of HONO in different regions in China.

4 Conclusions

This study for the first time systematically analyzed the production of HONO from the photolysis of particulate nitrate in $PM_{2.5}$ samples from multiple sites across China, shedding light to the contribution of this photolysis process to HONO daytime source in different environments. A total of 20 pairs of comparative photochemical experiments were conducted in Wangdu to evaluate and quantify the shadowing effect. We found that the corrected $J_{NO_3^-\text{-HONO}}$ values varied with sampling periods and locations over a wide range, distributing from 0.16×10^{-5} s^{-1} to 19.60 $\times10^{-5}$ s^{-1}. The coexisted organic components in $PM_{2.5}$ can promote the photolysis of particulate nitrate, with higher

$J_{NO_3^- - HONO}$ generally associated with higher OC/NO_3^- ratio. Considering the logarithmical decrease of $J_{NO_3^- - HONO}$ with increased NO_3^-, we suggested that the S_{HONO} should be calculated with $J_{NO_3^- - HONO}$ derived from the parameterization equation with OC/NO_3^- instead of the average value. The photolysis of particulate nitrate can become a potential daytime HONO source in southern urban cities, such as GuangZ, which was characterized by large VOCs emissions and enhanced formation of secondary particulate organic matter. Our work has provided an important reference for the research in other areas in the world with high proportion of organic components in aerosol samples, such as United States (Hass-Mitchell et al., 2024) and Europe (Bressi et al., 2021). To note, the filter samples collected in this work may not cover all representative environments in China, especially the background sites, more field observations and simulation experiments are needed in the future to better constrain the parameterization and mechanism of particulate nitrate photolysis.

Data availability. The data used in this paper can be provided upon request from the corresponding author.

Author contributions. J W, B L and K Z conceived the study and designed the experiments. **J W, B L, J G, C C, L W, Y Z, J L, Y Z, and X D** analyzed the data. **J W and B L** prepared the manuscript and all the coauthors helped improve the manuscript.

Competing interests. The authors declare that they have no conflict of interest.

Acknowledgement. We thank the Data Integration Program of the Major Research Plan of the National Natural Science Foundation of China (No. 92044303, https://www.capdatabase.cn) for making the high-resolution simulation dataset of $PM_{2.5}$ chemical composition in Chinese from 2013 to 2020 available.

Financial support. This work was supported by the Central Level, Scientific Research Institutes for Basic R&D Special Fund Business, China (No. 2022YSKY-26), and the National Key Research and Development Program of China (No. 2022YFC3701100).

References

Ammann, M., Kalberer, M., Jost, D. T., Tobler, L., Rössler, E., Piguet, D., Gäggeler, H. W., and Baltensperger, U.: Heterogeneous production of nitrous acid on soot in polluted air masses, Nature, 395, 157-160, 10.1038/25965, 1998.

Andersen, S. T., Carpenter, L. J., Reed, C., Lee, J. D., Chance, R., Sherwen, T., Vaughan, A. R., Stewart, J., Edwards, P. M., Bloss, W. J., Sommariva, R., Crilley, L. R., Nott, G. J., Neves, L., Read, K., Heard, D. E., Seakins, P. W., Whalley, L. K., Boustead, G. A., Fleming, L. T., Stone, D., and Fomba, K. W.: Extensive field evidence for the release of HONO from the photolysis of nitrate aerosols, Sci. Adv., 9, eadd6266, doi:10.1126/sciadv.add6266, 2023.

Atzei, D., Fermo, P., Vecchi, R., Fantauzzi, M., Comite, V., Valli, G., Cocco, F., and Rossi, A.: Composition and origin of $PM_{2.5}$ in Mediterranean Countryside, Environ. Pollut., 246, 294-302, https://doi.org/10.1016/j.envpol.2018.12.012, 2019.

Bao, F., Li, M., Zhang, Y., Chen, C., and Zhao, J.: Photochemical aging of Beijing urban $PM_{2.5}$: HONO production, Environ. Sci. Technol., 52, 6309-6316, 10.1021/acs.est.8b00538, 2018.

Bao, F., Jiang, H., Zhang, Y., Li, M., Ye, C., Wang, W., Ge, M., Chen, C., and Zhao, J.: The key role of sulfate in the photochemical renoxification on real $PM_{2.5}$, Environ. Sci. Technol., 54, 3121-3128, 10.1021/acs.est.9b06764, 2020.

Beine, H. J., Amoroso, A., Dominé, F., King, M. D., Nardino, M., Ianniello, A., and France, J. L.: Surprisingly small HONO emissions from snow surfaces at Browning Pass, Antarctica, Atmos. Chem. Phys., 6, 2569-2580, 10.5194/acp-6-2569-2006, 2006.

Bhattarai, H. R., Liimatainen, M., Nykänen, H., Kivimäenpää, M., Martikainen, P. J., and Maljanen, M.: Germinating wheat promotes the emission of atmospherically significant nitrous acid (HONO) gas from soils, Soil Biol. Biochem., 136, 10.1016/j.soilbio.2019.06.014, 2019.

Bressi, M., Cavalli, F., Putaud, J. P., Fröhlich, R., Petit, J. E., Aas, W., Äijälä, M., Alastuey, A., Allan, J. D., Aurela, M., Berico, M., Bougiatioti, A., Bukowiecki, N., Canonaco, F., Crenn, V., Dusanter, S., Ehn, M., Elsasser, M., Flentje, H., Graf, P., Green, D. C., Heikkinen, L., Hermann, H., Holzinger, R., Hueglin, C., Keernik, H., Kiendler-Scharr, A., Kubelová, L., Lunder, C., Maasikmets, M., Makeš, O., Malaguti, A., Mihalopoulos, N., Nicolas, J. B., O'Dowd, C., Ovadnevaite, J., Petralia, E., Poulain, L., Priestman, M., Riffault, V., Ripoll, A., Schlag, P., Schwarz, J., Sciare, J., Slowik, J., Sosedova, Y.,

528 Stavroulas, I., Teinemaa, E., Via, M., Vodička, P., Williams, P. I., Wiedensohler, A., Young, D. E.,
529 Zhang, S., Favez, O., Minguillón, M. C., and Prevot, A. S. H.: A European aerosol phenomenology -
530 7: High-time resolution chemical characteristics of submicron particulate matter across Europe,
531 Atmos. Environ.: X, 10, 10.1016/j.aeaoa.2021.100108, 2021.
532 Cao, Y., Ma, Q., Chu, B., and He, H.: Homogeneous and heterogeneous photolysis of nitrate in the
533 atmosphere: state of the science, current research needs, and future prospects, Front. Env. Sci. Eng.,
534 17, 10.1007/s11783-023-1648-6, 2022.
535 Chang, D., Wang, Z., Guo, J., Li, T., Liang, Y., Kang, L., Xia, M., Wang, Y., Yu, C., Yun, H., Yue, D.,
536 and Wang, T.: Characterization of organic aerosols and their precursors in southern China during a
537 severe haze episode in January 2017, Sci. Total. Environ., 691, 101-111,
538 10.1016/j.scitotenv.2019.07.123, 2019.
539 Cheng, C., Yang, S., Yuan, B., Pei, C., Zhou, Z., Mao, L., Liu, S., Chen, D., Cheng, X., Li, M., Shao,
540 M., and Zhou, Z.: The significant contribution of nitrate to a severe haze event in the winter of
541 Guangzhou, China, Sci. Total. Environ., 909, 168582, 10.1016/j.scitotenv.2023.168582, 2024.
542 Clegg, S. L., Brimblecombe, P., and Wexler, A. S.: Thermodynamic Model of the System
543 H^+–NH_4^+–Na^+–SO_4^{2-}–NO_3^-–Cl^-–H_2O at 298.15 K, J. Phy. Chem. A, 102, 2155-2171,
544 10.1021/jp973043j, 1998.
545 Finlayson-Pitts, B. J. a. P. J., J. N.: Chemistry of the upper and lower atmosphere: theory, experiments,
546 and applications, Academic Press, San Diego, CA, xxii+969 pp., ISBN 0-12-257060-x, 2000.
547 Fu, X., Wang, T., Zhang, L., Li, Q., Wang, Z., Xia, M., Yun, H., Wang, W., Yu, C., Yue, D., Zhou, Y.,
548 Zheng, J., and Han, R.: The significant contribution of HONO to secondary pollutants during a
549 severe winter pollution event in southern China, Atmos. Chem. Phys., 19, 1-14,
550 10.5194/acp-19-1-2019, 2019.
551 Gelencsér, A., Hoffer, A., Kiss, G., Tombácz, E., Kurdi, R., and Bencze, L.: In-situ formation of
552 light-absorbing organic matter in cloud water, J. Atmos. Chem., 45, 25-33,
553 10.1023/A:1024060428172, 2003.
554 Gen, M., Liang, Z., Zhang, R., Go Mabato, B. R., and Chan, C. K.: Particulate nitrate photolysis in the
555 atmosphere, Environ. Sci.-Atmos., 2, 111-127, 10.1039/d1ea00087j, 2022.
556 Gu, R., Shen, H., Xue, L., Wang, T., Gao, J., Li, H., Liang, Y., Xia, M., Yu, C., Liu, Y., and Wang, W.:
557 Investigating the sources of atmospheric nitrous acid (HONO) in the megacity of Beijing, China, Sci.

Total Environ., 812, 10.1016/j.scitotenv.2021.152270, 2022a.

Gu, R., Wang, W., Peng, X., Xia, M., Zhao, M., Zhang, Y., Wang, Y., Liu, Y., Shen, H., Xue, L., Wang, T., and Wang, W.: Nitrous acid in the polluted coastal atmosphere of the South China Sea: Ship emissions, budgets, and impacts, Sci. Total. Environ., 153692, 10.1016/j.scitotenv.2022.153692, 2022b.

Handley, S. R., Clifford, D., and Donaldson, D. J.: Photochemical loss of nitric acid on organic films: a possible recycling mechanism for NOx, Environ. Sci. Technol., 41, 3898-3903, 10.1021/es062044z, 2007.

Hass-Mitchell, T., Joo, T., Rogers, M., Nault, B. A., Soong, C., Tran, M., Seo, M., Machesky, J. E., Canagaratna, M., Roscioli, J., Claflin, M. S., Lerner, B. M., Blomdahl, D. C., Misztal, P. K., Ng, N. L., Dillner, A. M., Bahreini, R., Russell, A., Krechmer, J. E., Lambe, A., and Gentner, D. R.: Increasing contributions of temperature-dependent oxygenated organic aerosol to summertime particulate matter in New York City, ACS Environ. Sci. Technol. Air, 1, 113-128, 10.1021/acsestair.3c00037, 2024.

Hou, S., Tong, S., Ge, M., and An, J.: Comparison of atmospheric nitrous acid during severe haze and clean periods in Beijing, China, Atmos. Environ., 124, 199-206, 10.1016/j.atmosenv.2015.06.023, 2016.

Huang, R.., Yang, L., Cao, J., Wang, Q., Tie, X., Ho, K., Shen, Z., Zhang, R., Li, G., Zhu, C., Zhang, N., Dai, W., Zhou, J., Liu, S., Chen, Y., Chen, J., and O'Dowd, C. D.: Concentration and sources of atmospheric nitrous acid (HONO) at an urban site in Western China, Sci. Total Environ., 593-594, 165-172, https://doi.org/10.1016/j.scitotenv.2017.02.166, 2017.

Kim, M. and Or, D.: Microscale pH variations during drying of soils and desert biocrusts affect HONO and NH_3 emissions, Nat. Commun., 10, 3944, 10.1038/s41467-019-11956-6, 2019.

Kong, L., Tang, X., Zhu, J., Wang, Z., Liu, B., Zhu, Y., Zhu, L., Chen, D., Hu, K., Wu, H., Wu, Q., Shen, J., Sun, Y., Liu, Z., Xin, J., Ji, D., and Zheng, M.: High-resolution simulation dataset of hourly $PM_{2.5}$ chemical composition in China (CAQRA-aerosol) from 2013 to 2020, Adv. Atmos. Sci., 41, 1-16, 10.1007/s00376-024-4046-5, 2024.

Kurtenbach, R., Becker, K. H., Gomes, J. A. G., Kleffmann, J., Lörzer, J. C., Spittler, M., Wiesen, P., Ackermann, R., Geyer, A., and Platt, U.: Investigations of emissions and heterogeneous formation of HONO in a road traffic tunnel, Atmos. Environ., 35, 3385-3394,

588 https://doi.org/10.1016/S1352-2310(01)00138-8, 2001.
589 Lee, J. D., Whalley, L. K., Heard, D. E., Stone, D., Dunmore, R. E., Hamilton, J. F., Young, D. E.,
590 Allan, J. D., Laufs, S., and Kleffmann, J.: Detailed budget analysis of HONO in central London
591 reveals a missing daytime source, Atmos. Chem. Phys., 16, 2747-2764, 10.5194/acp-16-2747-2016,
592 2016.
593 Li, D., Xue, L., Wen, L., Wang, X., Chen, T., Mellouki, A., Chen, J., and Wang, W.: Characteristics and
594 sources of nitrous acid in an urban atmosphere of northern China: Results from 1-yr continuous
595 observations, Atmos. Environ., 182, 296-306, https://doi.org/10.1016/j.atmosenv.2018.03.033, 2018.
596 Li, W., Tong, S., Cao, J., Su, H., Zhang, W., Wang, L., Jia, C., Zhang, X., Wang, Z., Chen, M., and Ge,
597 M.: Comparative observation of atmospheric nitrous acid (HONO) in Xi'an and Xianyang located in
598 the GuanZhong basin of western China, Environ. Pollut., 289, 117679,
599 10.1016/j.envpol.2021.117679, 2021.
600 Li, X., Brauers, T., Häseler, R., Bohn, B., Fuchs, H., Hofzumahaus, A., Holland, F., Lou, S., Lu, K. D.,
601 Rohrer, F., Hu, M., Zeng, L. M., Zhang, Y. H., Garland, R. M., Su, H., Nowak, A., Wiedensohler, A.,
602 Takegawa, N., Shao, M., and Wahner, A.: Exploring the atmospheric chemistry of nitrous acid
603 (HONO) at a rural site in Southern China, Atmos. Chem. Phys., 12, 1497-1513,
604 10.5194/acp-12-1497-2012, 2012.
605 Li, Y., An, J., Min, M., Zhang, W., Wang, F., and Xie, P.: Impacts of HONO sources on the air quality
606 in Beijing, Tianjin and Hebei Province of China, Atmos. Environ., 45, 4735-4744,
607 https://doi.org/10.1016/j.atmosenv.2011.04.086, 2011.
608 Li, Z., Ren, Z., Liu, C., Ning, Z., Liu, J., Liu, J., Zhai, Z., Ma, X., Chen, L., Zhang, Y., Bai, L., and
609 Kong, S.: Heterogeneous variations in wintertime $PM_{2.5}$ sources, compositions and exposure risks at
610 urban/suburban rural/remote rural areas in the post COVID-19/Clean-Heating period, Atmos.
611 Environ., 326, 120463, https://doi.org/10.1016/j.atmosenv.2024.120463, 2024.
612 Lian, C., Wang, W., Chen, Y., Zhang, Y., Zhang, J., Liu, Y., Fan, X., Li, C., Zhan, J., Lin, Z., Hua, C.,
613 Zhang, W., Liu, M., Li, J., Wang, X., An, J., and Ge, M.: Long-term winter observation of nitrous
614 acid in the urban area of Beijing, J. Environ. Sci. (China), 114, 334-342, 10.1016/j.jes.2021.09.010,
615 2022.
616 Liang, Y., Zha, Q., Wang, W., Cui, L., Lui, K. H., Ho, K. F., Wang, Z., Lee, S., and Wang, T.: Revisiting
617 nitrous acid (HONO) emission from on-road vehicles: A tunnel study with a mixed fleet, J. Air Waste

618 Manage., 67, 797-805, 10.1080/10962247.2017.1293573, 2017.
619 Liao, S., Zhang, J., Yu, F., Zhu, M., Liu, J., Ou, J., Dong, H., Sha, Q., Zhong, Z., Xie, Y., Luo, H.,
620 Zhang, L., and Zheng, J.: High gaseous nitrous acid (HONO) emissions from light-duty diesel
621 vehicles, Environ. Sci. Technol., 55, 200-208, 10.1021/acs.est.0c05599, 2021.
622 Liu, P., Zhang, C., Mu, Y., Liu, C., Xue, C., Ye, C., Liu, J., Zhang, Y., and Zhang, H.: The possible
623 contribution of the periodic emissions from farmers' activities in the North China Plain to
624 atmospheric water-soluble ions in Beijing, Atmos. Chem. Phys., 16, 10097-10109,
625 10.5194/acp-16-10097-2016, 2016.
626 Liu, P., Zhang, C., Xue, C., Mu, Y., Liu, J., Zhang, Y., Tian, D., Ye, C., Zhang, H., and Guan, J.: The
627 contribution of residential coal combustion to atmospheric $PM_{2.5}$ in northern China during winter,
628 Atmos. Chem. Phys., 17, 11503-11520, 10.5194/acp-17-11503-2017, 2017.
629 Liu, Y., Lu, K., Li, X., Dong, H., Tan, Z., Wang, H., Zou, Q., Wu, Y., Zeng, L., Hu, M., Min, K.-E.,
630 Kecorius, S., Wiedensohler, A., and Zhang, Y.: A comprehensive model test of the HONO sources
631 constrained to field measurements at rural North China Plain, Environ. Sci. Technol., 53, 3517-3525,
632 10.1021/acs.est.8b06367, 2019.
633 Melissa A, D.: Soil surface acidity plays a determining role in the atmospheric-terrestrial exchange of
634 nitrous acid, Proc. Natl. Acad. Sci. U. S. A., 52, 18472-18477, 10.1073/pnas.1418545112, 2014.
635 Monge, M. E., D'Anna, B., Mazri, L., Giroir-Fendler, A., Ammann, M., Donaldson, D. J., and George,
636 C.: Light changes the atmospheric reactivity of soot, Proc. Natl. Acad. Sci. U. S. A., 107, 6605-6609,
637 10.1073/pnas.0908341107, 2010.
638 Mora Garcia, S. L., Pandit, S., Navea, J. G., and Grassian, V. H.: Nitrous acid (HONO) formation from
639 the irradiation of aqueous nitrate solutions in the presence of marine chromophoric dissolved organic
640 matter: comparison to other organic photosensitizers, ACS Earth Space Chem., 5, 3056-3064,
641 10.1021/acsearthspacechem.1c00292, 2021.
642 Oswald, R., Behrendt, T., Ermel, M., Wu, D., Su, H., Cheng, Y., Breuninger, C., Moravek, A., Mougin,
643 E., Delon, C., Loubet, B., Pommerening-Roser, A., Sorgel, M., Poschl, U., Hoffmann, T., Andreae,
644 M. O., Meixner, F. X., and Trebs, I.: HONO emissions from soil bacteria as a major source of
645 atmospheric reactive nitrogen, Science, 341, 1233-1235, 10.1126/science.1242266, 2013.
646 Pipalatkar, P., Khaparde, V. V., Gajghate, D. G., and Bawase, M. A.: Source apportionment of $PM_{2.5}$
647 using a CMB model for a centrally located Indian city, Aerosol Air Qual. Res., 14, 1089-1099,

10.4209/aaqr.2013.04.0130, 2014.

Reeser, D. I., Kwamena, N.-O. A., and Donaldson, D. J.: Effect of organic coatings on gas-phase nitrogen dioxide production from aqueous nitrate photolysis, J. Phys. Chem. C, 117, 22260-22267, 10.1021/jp401545k, 2013.

Ren, X., Harder, H., Martinez, M., Lesher, R. L., Oliger, A., Simpas, J. B., Brune, W. H., Schwab, J. J., Demerjian, K. L., He, Y., Zhou, X., and Gao, H.: OH and HO_2 Chemistry in the urban atmosphere of New York City, Atmos. Environ., 37, 3639-3651, https://doi.org/10.1016/S1352-2310(03)00459-X, 2003.

Romer, P. S., Wooldridge, P. J., Crounse, J. D., Kim, M. J., Wennberg, P. O., Dibb, J. E., Scheuer, E., Blake, D. R., Meinardi, S., Brosius, A. L., Thames, A. B., Miller, D. O., Brune, W. H., Hall, S. R., Ryerson, T. B., and Cohen, R. C.: Constraints on aerosol nitrate photolysis as a potential source of HONO and NOx, Environ. Sci. Technol., 52, 13738-13746, 10.1021/acs.est.8b03861, 2018.

Scharko, N. K., Berke, A. E., and Raff, J. D.: Release of nitrous acid and nitrogen dioxide from nitrate photolysis in acidic aqueous solutions, Environ. Sci. Technol., 48, 11991-12001, 10.1021/es503088x, 2014.

Shi, Q., Tao, Y., Krechmer, J. E., Heald, C. L., Murphy, J. G., Kroll, J. H., and Ye, Q.: Laboratory investigation of renoxification from the photolysis of inorganic particulate nitrate, Environ. Sci. Technol., 55, 854-861, 10.1021/acs.est.0c06049, 2021.

Slater, E. J., Whalley, L. K., Woodward-Massey, R., Ye, C., Lee, J. D., Squires, F., Hopkins, J. R., Dunmore, R. E., Shaw, M., Hamilton, J. F., Lewis, A. C., Crilley, L. R., Kramer, L., Bloss, W., Vu, T., Sun, Y., Xu, W., Yue, S., Ren, L., Acton, W. J. F., Hewitt, C. N., Wang, X., Fu, P., and Heard, D. E.: Elevated levels of OH observed in haze events during wintertime in central Beijing, Atmos. Chem. Phys., 20, 14847-14871, 10.5194/acp-20-14847-2020, 2020.

Stemmler, K., Ammann, M., Donders, C., Kleffmann, J., and George, C.: Photosensitized reduction of nitrogen dioxide on humic acid as a source of nitrous acid, Nature, 440, 195-198, 10.1038/nature04603, 2006.

Su, H., Cheng, Y. F., Shao, M., Gao, D. F., Yu, Z. Y., Zeng, L. M., Slanina, J., Zhang, Y. H., and Wiedensohler, A.: Nitrous acid (HONO) and its daytime sources at a rural site during the 2004 PRIDE-PRD experiment in China, J. Geophys. Res. Atmos., 113, 10.1029/2007jd009060, 2008.

Su, H., Cheng, Y., Oswald, R., Behrendt, T., Trebs, I., Meixner, F. X., Andreae, M. O., Cheng, P., Zhang,

678 Y., and Poschl, U.: Soil nitrite as a source of atmospheric HONO and OH radicals, Science, 333,
679 1616-1618, 10.1126/science.1207687, 2011.
680 Svoboda, O., Kubelová, L., and Slavíček, P.: Enabling forbidden processes: quantum and solvation
681 enhancement of nitrate anion UV absorption, J. Phys. Chem. A, 117, 12868-12877,
682 10.1021/jp4098777, 2013.
683 Villena, G., Wiesen, P., Cantrell, C. A., Flocke, F., Fried, A., Hall, S. R., Hornbrook, R. S., Knapp, D.,
684 Kosciuch, E., Mauldin, R. L., McGrath, J. A., Montzka, D., Richter, D., Ullmann, K., Walega, J.,
685 Weibring, P., Weinheimer, A., Staebler, R. M., Liao, J., Huey, L. G., and Kleffmann, J.: Nitrous acid
686 (HONO) during polar spring in Barrow, Alaska: A net source of OH radicals?, J. Geophys. Res., 116,
687 10.1029/2011jd016643, 2011.
688 Wang, H., Ding, J., Xu, J., Wen, J., Han, J., Wang, K., Shi, G., Feng, Y., Ivey, C. E., Wang, Y., Nenes,
689 A., Zhao, Q., and Russell, A. G.: Aerosols in an arid environment: The role of aerosol water content,
690 particulate acidity, precursors, and relative humidity on secondary inorganic aerosols, Sci. Total
691 Environ., 646, 564-572, https://doi.org/10.1016/j.scitotenv.2018.07.321, 2019.
692 Wang, J., Zhang, X., Guo, J., Wang, Z., and Zhang, M.: Observation of nitrous acid (HONO) in Beijing,
693 China: Seasonal variation, nocturnal formation and daytime budget, Sci. Total Environ., 587-588,
694 350-359, 10.1016/j.scitotenv.2017.02.159, 2017.
695 Wang, J., Gao, J., Che, F., Wang, Y., Lin, P., and Zhang, Y.: Decade-long trends in chemical component
696 properties of $PM_{2.5}$ in Beijing, China (2011-2020), Sci. Total Environ., 832, 154664,
697 10.1016/j.scitotenv.2022.154664, 2022a.
698 Wang, J., Gao, J., Che, F., Wang, Y., Lin, P., and Zhang, Y.: Dramatic changes in aerosol composition
699 during the 2016-2020 heating seasons in Beijing-Tianjin-Hebei region and its surrounding areas: The
700 role of primary pollutants and secondary aerosol formation, Sci. Total. Environ., 849, 157621,
701 10.1016/j.scitotenv.2022.157621, 2022b.
702 Wang, J., Zhang, Y., Zhang, C., Wang, Y., Zhou, J., Whalley, L. K., Slater, E. J., Dyson, J. E., Xu, W.,
703 Cheng, P., Han, B., Wang, L., Yu, X., Wang, Y., Woodward-Massey, R., Lin, W., Zhao, W., Zeng, L.,
704 Ma, Z., Heard, D. E., and Ye, C.: Validating HONO as an intermediate tracer of the external cycling
705 of reactive nitrogen in the background atmosphere, Environ. Sci. Technol., 57, 5474-5484,
706 10.1021/acs.est.2c06731, 2023a.
707 Wang, Y., Fu, X., Wang, T., Ma, J., Gao, H., Wang, X., and Pu, W.: Large contribution of nitrous acid to

soil-emitted reactive oxidized nitrogen and its effect on air quality, Environ. Sci. Technol., 57, 3516-3526, 10.1021/acs.est.2c07793, 2023b.

Wang, Y., Xiao, S., Zhang, Y., Chang, H., Martin, R. V., Van Donkelaar, A., Gaskins, A., Liu, Y., Liu, P., and Shi, L.: Long-term exposure to $PM_{2.5}$ major components and mortality in the southeastern United States, Environ. Int., 158, 106969, 10.1016/j.envint.2021.106969, 2022c.

Wang, Y., Huang, D. D., Huang, W., Liu, B., Chen, Q., Huang, R., Gen, M., Mabato, B. R. G., Chan, C. K., Li, X., Hao, T., Tan, Y., Hoi, K. I., Mok, K. M., and Li, Y. J.: Enhanced nitrite production from the aqueous photolysis of nitrate in the presence of vanillic acid and implications for the roles of light-absorbing organics, Environ. Sci. Technol., 55, 15694-15704, 10.1021/acs.est.1c04642, 2021.

Wang, Z., Zhang, D., Liu, B., Li, Y., Chen, T., Sun, F., Yang, D., Liang, Y., Chang, M., Yang, L., and Lin, A.: Analysis of chemical characteristics of $PM_{2.5}$ in Beijing over a 1-year period, J. Atmos. Chem., 73, 407-425, 10.1007/s10874-016-9334-8, 2016.

Wexler, A. S. and Clegg, S. L.: Atmospheric aerosol models for systems including the ions H^+, NH_4^+, Na^+, SO_4^{2-}, NO_3^-, Cl^-, Br^-, and H_2O, J. Geophys. Res. Atmos., 107, ACH 14-1-ACH 14-14, https://doi.org/10.1029/2001JD000451, 2002.

Xiao, H. W., Xiao, H. Y., Luo, L., Shen, C. Y., Long, A. M., Chen, L., Long, Z. H., and Li, D. N.: Atmospheric aerosol compositions over the South China Sea: temporal variability and source apportionment, Atmos. Chem. Phys., 17, 3199-3214, 10.5194/acp-17-3199-2017, 2017.

Yang, W., Han, C., Yang, H., and Xue, X.: Significant HONO formation by the photolysis of nitrates in the presence of humic acids, Environ. Pollut., 243, 679-686, 10.1016/j.envpol.2018.09.039, 2018.

Ye, C., Gao, H., Zhang, N., and Zhou, X.: Photolysis of nitric acid and nitrate on natural and artificial surfaces, Environ. Sci. Technol., 50, 3530-3536, 10.1021/acs.est.5b05032, 2016a.

Ye, C., Zhang, N., Gao, H., and Zhou, X.: Photolysis of particulate nitrate as a source of HONO and NOx, Environ. Sci. Technol., 51, 6849-6856, 10.1021/acs.est.7b00387, 2017.

Ye, C., Zhang, N., Gao, H., and Zhou, X.: Matrix effect on surface-catalyzed photolysis of nitric acid, Sci. Rep., 9, 4351, 10.1038/s41598-018-37973-x, 2019.

Ye, C., Zhou, X., Pu, D., Stutz, J., Festa, J., Spolaor, M., Tsai, C., Cantrell, C., Mauldin, R. L., Campos, T., Weinheimer, A., Hornbrook, R. S., Apel, E. C., Guenther, A., Kaser, L., Yuan, B., Karl, T., Haggerty, J., Hall, S., Ullmann, K., Smith, J. N., Ortega, J., and Knote, C.: Rapid cycling of reactive nitrogen in the marine boundary layer, Nature, 532, 489-491, 10.1038/nature17195, 2016b.

738 Zhang, L., Wang, T., Zhang, Q., Zheng, J., Xu, Z., and Lv, M.: Potential sources of nitrous acid (HONO)
739 and their impacts on ozone: A WRF-Chem study in a polluted subtropical region, J. Geophys. Res.
740 Atmos., 121, 3645-3662, https://doi.org/10.1002/2015JD024468, 2016.
741 Zhang, R., Gen, M., Huang, D., Li, Y., and Chan, C. K.: Enhanced sulfate production by nitrate
742 photolysis in the presence of halide ions in atmospheric particles, Environ. Sci. Technol., 54,
743 3831-3839, 10.1021/acs.est.9b06445, 2020a.
744 Zhang, W., Tong, S., Jia, C., Wang, L., Liu, B., Tang, G., Ji, D., Hu, B., Liu, Z., Li, W., Wang, Z., Liu,
745 Y., Wang, Y., and Ge, M.: Different HONO sources for three layers at the urban area of Beijing,
746 Environ. Sci. Technol., 54, 12870-12880, 10.1021/acs.est.0c02146, 2020b.
747 Zheng, J., Shao, M., Che, W., Zhang, L., Zhong, L., Zhang, Y., and Streets, D.: Speciated VOC
748 emission inventory and spatial patterns of ozone formation potential in the Pearl River Delta, China,
749 Environ. Sci. Technol., 43, 8580-8586, 10.1021/es901688e, 2009.
750 Zhou, X., Gao, H., He, Y., Huang, G., Bertman, S. B., Civerolo, K., and Schwab, J.: Nitric acid
751 photolysis on surfaces in low-NOx environments: Significant atmospheric implications, Geophys.
752 Res. Let., 30, https://doi.org/10.1029/2003GL018620, 2003.
753 Zhou, X., Zhang, N., TerAvest, M., Tang, D., Hou, J., Bertman, S., Alaghmand, M., Shepson, P. B.,
754 Carroll, M. A., Griffith, S., Dusanter, S., and Stevens, P. S.: Nitric acid photolysis on forest canopy
755 surface as a source for tropospheric nitrous acid, Nat. Geosci., 4, 440-443, 10.1038/ngeo1164, 2011.